

Proton driver optimization for new generation neutrino superbeams to search for sub-leading $\nu_\mu \rightarrow \nu_e$ oscillations (θ_{13} angle)

A. Ferrari^{a,1}, A. Rubbia^b, C. Rubbia^c and P.R. Sala^{b,1}

a) CERN, Geneva, Switzerland

b) Institut für Teilchenphysik, ETHZ, CH-8093 Zürich, Switzerland

c) ENEA and Pavia University, Italy

Abstract

In this paper, we perform a systematic study of particle production and neutrino yields for different incident proton energies E_p and baselines L , with the aim of optimizing the parameters of a neutrino beam for the investigation of θ_{13} -driven neutrino oscillations in the Δm^2 range allowed by Superkamiokande results. We study the neutrino energy spectra in the “relevant” region of the first maximum of the oscillation at a given baseline L . We find that to each baseline L corresponds an “optimal” proton energy E_p which minimizes the required integrated proton intensity needed to observe a fixed number of oscillated events. In addition, we find that the neutrino event rate in the relevant region scales approximately linearly with the proton energy. Hence, baselines L and proton energies E_p can be adjusted and the performance for neutrino oscillation searches will remain approximately unchanged provided that the product of the proton energy times the number of protons on target remains constant. We apply these ideas to the specific cases of 2.2, 4.4, 20, 50 and 400 GeV protons. We simulate focusing systems that are designed to best capture the secondary pions of the “optimal” energy. We compute the expected sensitivities to $\sin^2 2\theta_{13}$ for the various configurations by assuming the existence of new generation accelerators able to deliver integrated proton intensities on target times the proton energy of the order of $\mathcal{O}(5 \times 10^{23})$ GeV \times pot/year.

1 Introduction

The firmly established disappearance of muon neutrinos of cosmic ray origin [1, 2] strongly points toward the existence of neutrino oscillations [3].

¹On leave of absence from INFN Milano.

The approved first generation long baseline (LBL) experiments — K2K [4], MINOS [5], ICARUS [6] and OPERA [7] — will search for a conclusive and unambiguous signature of the oscillation mechanism. They will provide the first precise measurements of the parameters governing the main muon disappearance mechanism. In particular, the CERN-NGS beam[8, 9], specifically optimized for tau appearance, will allow to directly confirm the hints for neutrino flavor oscillation.

In addition to the dominant $\nu_\mu \rightarrow \nu_\tau$ oscillation, it is possible that a sub-leading transition involving electron-neutrinos occur as well. In the “standard interpretation” of the 3-neutrino mixing, the $\nu_\mu \rightarrow \nu_e$ oscillations at the $\Delta m^2 \approx 2.5 \times 10^{-3} \text{ eV}^2$ indicated by atmospheric neutrinos is driven by the so-called θ_{13} angle. Indeed, given the flavor eigenstates $\nu_\alpha (\alpha = e, \mu, \tau)$ related to the mass eigenstates $\nu'_i (i = 1, 2, 3)$ where $\nu_\alpha = U_{\alpha i} \nu'_i$, the mixing matrix U is parameterized as:

$$U(\theta_{12}, \theta_{13}, \theta_{23}, \delta) = \begin{pmatrix} c_{12}c_{13} & s_{12}c_{13} & s_{13}e^{-i\delta} \\ -s_{12}c_{23} - c_{12}s_{13}s_{23}e^{i\delta} & c_{12}c_{23} - s_{12}s_{13}s_{23}e^{i\delta} & c_{13}s_{23} \\ s_{12}s_{23} - c_{12}s_{13}c_{23}e^{i\delta} & -c_{12}s_{23} - s_{12}s_{13}c_{23}e^{i\delta} & c_{13}c_{23} \end{pmatrix} \quad (1)$$

with $s_{ij} = \sin \theta_{ij}$ and $c_{ij} = \cos \theta_{ij}$.

The best sensitivity for this oscillation is expected for ICARUS at the CERN-NGS. Limited by the CNGS beam statistics at low energy, this search should allow to improve by roughly a factor 5 (see Ref.[6]) the CHOOZ[10] limit on the θ_{13} angle for $\Delta m^2 \approx 3 \times 10^{-3} \text{ eV}^2$. Beyond this program, new methods will be required in order to improve significantly the sensitivity.

At present, the only well established proposal in this direction is the JHF-Kamioka project[11]. In its first phase, 5 years of operation with the Super-K detector, it aims to a factor 20 improvement over the CHOOZ limit.

In Ref.[12], we have studied an optimization of the CNGS optics that would allow to increase the neutrino flux yield at low energy by a factor 5 compared to the baseline τ -optimization of the CNGS beam. This would yield an improvement in the sensitivity by about a factor two, or equivalently an improvement of a factor 10 compared to CHOOZ.

In this paper, FLUKA[13, 14] Monte Carlo simulations are employed to perform a systematic study of particle production and neutrino yields for different beam energy and baselines. Focusing systems adapted to the low energy range are also investigated, to obtain realistic estimates of the achievable neutrino rates.

The whole procedure is assumed to be detector and accelerator independent. Nevertheless, to give a first estimate of the needed beam intensities, the ICARUS T3000 detector size has been assumed as a reference. This is also justified by a recent neutrino detector comparison[15], following which the 2.35 kton LAr ICARUS fiducial mass is equivalent to a detector of approximately 20 kton of steel or 50 kton of water. For this reason, we concentrate on the intrinsic electron-neutrino background from the beam and do not explicitly calculate other sources of backgrounds that are strongly related

to detector performances, such as backgrounds from π^0 production in neutral current events . We assume that in reality the “best” beam would be complemented by the “best” detector and that these backgrounds will only introduce a small correction to our sensitivity estimates. In addition, we are primarily interested at this stage in the comparison among proton drivers.

We consider so-called “conventional” neutrino superbeams, in which neutrinos are produced by the decay of secondary pions obtained in high-energy collisions of protons on an appropriate target and followed by a magnetic focusing system.

In this kind of beams, the neutrino beam spectrum and its flux are essentially determined by three parameters that can be optimized appropriately:

- the primary proton energy E_p ,
- the number of protons on target N_{pot} per year,
- the focusing system, which focus a fraction of the secondary charged pions and kaons (positive or both signs depending on the focusing device).

In order to simplify the problem, we consider three “classes” of proton energies:

- *Low energy*: protons in a range of a few GeV. We take as reference the CERN-SPL proton driver design[16] with 2.2 GeV kinetic energy and an “upgraded SPL” with similar characteristics but with 4.4 GeV protons;
- *Medium energy*: we take 20 GeV proton energy, similar to the CERN PS machine and the 50 GeV of the JHF facility[11];
- *High-energy*: we take the highest energies, i.e. the 400 GeV protons like in the case of the CERN SPS.

The purpose of this work is to understand the required intensities for the various proton energies, in other words, is it more favorable to employ low-energy, high-intensity proton or high-energy, low-intensity proton machines?

2 Observing the oscillation – choosing L and E

In order to maximize the probability of an oscillation, we must choose the energy of the neutrino E_{max} and the baseline L such that

$$1.27 \frac{L(km)}{E_{max}(GeV)} \Delta m^2 (eV^2) \simeq \frac{\pi}{2} \quad (2)$$

However, in order to *observe the oscillation*, we must at least see the maximum preceded by a minimum, given by

$$1.27 \frac{L(\text{km})}{E_{\min}(\text{GeV})} \Delta m^2(\text{eV}^2) \simeq \pi \quad (3)$$

The mass difference indicated by Superkamiokande is given by $\Delta m^2 \approx 2.5 \times 10^{-3} \text{ eV}^2$ and lies within the range $1 \times 10^{-3} < \Delta m^2 < 4 \times 10^{-3} \text{ eV}^2$ [17].

Since we are considering one single detector at a given location as target, our baseline L for a given source is fixed. This implies that *the neutrino beam spectrum should not be too narrow*, e.g. it should be a relatively wide-band beam in order to cope with the uncertainty on the Δm^2 . Since the knowledge on this parameter will improve with time, in particular with the running of K2K, MINOS and CNGS experiments, the range of energies will eventually be limited by the desire to observe the minimum and the maximum. In the meantime, we consider the full mass range indicated by atmospheric neutrino observation.

We do not wish to consider baselines longer than the current CNGS baseline of $L = 730 \text{ km}$ and use therefore a range of baselines between 100 km and 730 km. Table 1 shows the values (in MeV) of E_{\min} and E_{\max} defined above as a function for the baselines. The energies range from about 50 MeV to 300 MeV for $L = 100 \text{ km}$ and from 300 MeV to 2400 MeV for $L = 730 \text{ km}$. Clearly, we wish to optimize for high intensity, low energy neutrino superbeams.

We note that at these low energies, neutrino interactions are clearly identifiable and have generally easily reconstructible final-states. This is an advantage for detector-related background suppression. In a detector with the granularity like ICARUS, neutral pions can be easily suppressed via energy ionization or by direct reconstruction of the two (well separated) decay photons.

3 The approximate scaling with proton energy

The understanding of the relationship between primary beam energy and neutrino production is the first step toward any optimization. To isolate this relationship from the other parameters, it is more convenient to work in the “perfect focusing” approximation, where *all (positively charged) mesons produced within a given solid angle* are supposed to be focused exactly on the detector direction¹. In our case, we set $P_T = 0$ for all secondary positively charged particles produced within 1 rad.

All the simulations presented in this section have been performed with the same target and decay tunnel geometry. The target is in graphite, density 1.8 g/cm^3 , one

¹In order to derive the scaling, we consider only neutrino fluxes. However, in Section 6, when we compute our oscillation sensitivities we shall include both neutrinos and antineutrinos components obtained from the full simulation of the mesons of the relevant charge.

| L (km) | $\Delta m^2 (\text{eV}^2)$ | | | | | | | |
|-----------|----------------------------|------------------|--------------------|------------------|--------------------|------------------|--------------------|------------------|
| | 1×10^{-3} | | 2×10^{-3} | | 3×10^{-3} | | 4×10^{-3} | |
| | E_{max} MeV | E_{min} MeV | E_{max} MeV | E_{min} MeV | E_{max} MeV | E_{min} MeV | E_{max} MeV | E_{min} MeV |
| 100 | 81 | 40 | 162 | 81 | 243 | 121 | 323 | 162 |
| 150 | 121 | 61 | 243 | 121 | 364 | 182 | 485 | 243 |
| 200 | 162 | 81 | 323 | 162 | 485 | 243 | 647 | 323 |
| 300 | 243 | 121 | 485 | 243 | 728 | 364 | 970 | 485 |
| 400 | 323 | 162 | 647 | 323 | 970 | 485 | 1294 | 647 |
| 500 | 404 | 202 | 809 | 404 | 1213 | 606 | 1617 | 809 |
| 600 | 485 | 243 | 970 | 485 | 1455 | 728 | 1940 | 970 |
| 730 | 590 | 295 | 1180 | 590 | 1771 | 885 | 2361 | 1180 |

Table 1: Neutrino energies E_{max} and E_{min} (see text for definition) corresponding to the maximum and minimum of the $\nu_\mu \rightarrow \nu_x$ oscillation for various baselines and the Δm^2 range indicated by Superkamiokande.

meter long, 2 mm radius; the decay tunnel is 150 m long and 3.5 m in radius. Target optimization will not change the general scaling, and the effect of the tunnel length on muon neutrino production can be accounted for in first approximation assuming that all neutrinos are produced by pions, and that they carry the maximum possible momentum.

The pion production rate at the exit of the target for various incident proton energies E_p as estimated with FLUKA are shown in Figure 1 for energies ranging from 2.2 GeV up to the 400 GeV of the SPS for the CNGS beam. In order to compare pion productions at different proton energies, we *divide the spectra by the proton energy E_p* .

All normalized spectra have similar shape, with the maximum yield at low energies ($p_\pi \approx 500$ MeV). Far from the endpoint, all spectra scale approximately with the incoming proton energy. Departures from the overall scaling consist in a slightly different shape at low E_p , and harder spectra at high E_p .

If the detector is far away in the forward direction, the neutrino event rate as a function of neutrino energy can be derived from these spectra by considering that:

- The neutrino carries a momentum that is 0.43 times the parent pion momentum
- The Lorentz boost gives a factor proportional to $E_\pi^2 \propto E_\nu^2$ on the solid angle
- The neutrino cross section grows approximately as E_ν (not true at the lowest energies, where the quasi-elastic grows more rapidly, however, for the optimization of the proton energy, this approximation is adequate.)

For a given E_ν , these factors apply *independently* on the primary proton energy. Thus, we expect that the energy scaling observed on the pion production is reflected

in the neutrino production. This is shown in Figure 2, where we plot the simulated muon neutrino event rate scaled with the primary proton energy.

The super-position of the curves at the lowest energies is impressive, except for one at $E_p = 400$ GeV. Of course, by rising E_p the energy-integrated event rate raises dramatically because the spectra extend to higher energies, but the event rate for a given $E_\nu < \approx 0.15 \times E_p$ is simply proportional to E_p .

This approximate scaling implies that we can define a *power factor* \mathcal{F} for neutrino production as the product of the proton energy times the beam intensity:

$$\mathcal{F} = E_p \times N_{pot} \quad (4)$$

Up to now we did not take into account the neutrino oscillation probability. If the aim is that of having a neutrino beam centered on the oscillation maximum, E_ν and the baseline L have to be chosen such as

$$\sin^2 \left(1.27 \Delta m^2 \frac{L}{E_\nu} \right) \approx 1, \quad (5)$$

thus

$$E_{max} \propto L. \quad (6)$$

How to choose the baseline L to maximize the rate of oscillated neutrino events per proton incident on the neutrino target? The neutrino flux grows scales like $1/L^2$, like the solid angle. But L and E_{max} are proportional, thus dividing bin by bin the simulated neutrino spectra with a factor E_ν^2 one gets the shape of the event rate as a function of E_{max} . This has been done for the perfect focusing approximation in Figure 3 for various proton energies E_p .

It is evident that the most optimal situation is for E_{max} in the range 200-600 MeV and *this results holds essentially independently of the proton energy*, at least as long as we discard the very high 400 GeV energy case. We can go beyond the $1/E_\nu^2$ approximation and in the following we will use the exact expression for the oscillation probability and will compute exactly the number of oscillated events by folding the expected neutrino spectra.

Nonetheless, the situation gives us a large freedom in the choice of proton energy, *provided that the intensity can be re-scaled accordingly*, so that the power factor remains essentially constant

$$\mathcal{F} = E_p \times N_{pot} \approx const. \quad (7)$$

4 The optimal baseline L for each proton energy

In order to study the scaling with the proton energy E_p and the baseline L , we compute the number N_e of oscillated $\nu_\mu \rightarrow \nu_e$ events:

$$N_e \propto \mathcal{I}_{pot} \int_0^\infty dE_\nu \sigma(E_\nu) \phi(E_\nu) P(\nu_\mu \rightarrow \nu_e, E_\nu, L, \Delta m^2, \sin^2 2\theta_{13}) \quad (8)$$

where $\phi(E_\nu)$ is the neutrino flux per proton on target. We normalize this number to a 2.35 kton (argon) detector, and assume 100% electron detection efficiency. For definiteness, we assume unless otherwise noted that $\Delta m^2 = 3 \times 10^{-3} \text{ eV}^2$ and $\sin^2 2\theta_{13} = 1 \times 10^{-3}$.

In order to take into account the effect of focusing (realistic focusing is discussed in section 5), we focus ideally all particles with the acceptance of 1 rad and apply a constant “focusing efficiency” of 20%, i.e. scale down the rates by a factor 5. We will see that this assumption is quite realistic and at least conservative for the low energy neutrinos.

Similarly, one can also estimate the “goodness” of the neutrino flux by computing the number of muon charged current events $N_{\mu,CC}^0$ within the energies $E_{min}(\Delta m^2 = 1 \times 10^{-3} \text{ eV}^2)$ and $E_{max}(\Delta m^2 = 4 \times 10^{-3} \text{ eV}^2)$ (see Table 1) of the oscillation:

$$N_{\mu,CC}^0 \propto \int_{E_{min}}^{E_{max}} dE_\nu \sigma(E_\nu) \phi(E_\nu) \quad (9)$$

We choose to normalize $N_{\mu,CC}^0$ to 10^{19} pots and per kton of (argon) target.

With these two parameters, we can easily compare all the possible options. It is fair to note that the number of oscillated events N_e assumes that the search is not limited by background, which in practice is *not* the case, as we will show in section 6. However, we prefer to separate the issue of background (which will be discussed in section 7) and concentrate for the moment on the question of the needed proton intensity. As we will show, the background turns out to be also quite independent of the proton energy and hence it does not enter in the optimization of the proton energy.

The results as a function of the baseline L are summarized in Table 2. The configuration corresponding to the minimum \mathcal{I}_{pot} is shown in bold.

We observe that *for each baseline there is an optimal proton energy $E_p^{optimal}$, which minimizes the required integrated proton intensity \mathcal{I}_{pot} to observe a fixed number of oscillated events.* This is also visible in Figure 8, where we plot the integrated beam intensity needed to obtain 5 oscillated ν_e events in a 2.35 kton detector for $\Delta m^2 = 3 \times 10^{-3} \text{ eV}^2$ and $\sin^2(2\theta_{13}) = 10^{-3}$ for different beam energies and baselines. The point of minimum pots corresponds approximately to the maximum ν_μ event rate.

This is because in that point, the secondary pion yield energy spectrum per proton on target, is best matched to the neutrino oscillation probability. Conversely, for

| L km | 2.2 GeV | | 4.4 GeV | | 20 GeV | | 50 GeV | | 400 GeV | |
|---------|----------------|---------------------------------------|----------------|---------------------------------------|----------------|---------------------------------------|----------------|---------------------------------------|----------------|---------------------------------------|
| | $N_{\mu,CC}^0$ | \mathcal{I}_{pot} | $N_{\mu,CC}^0$ | \mathcal{I}_{pot} | $N_{\mu,CC}^0$ | \mathcal{I}_{pot} | $N_{\mu,CC}^0$ | \mathcal{I}_{pot} | $N_{\mu,CC}^0$ | \mathcal{I}_{pot} |
| 100 | 0.035 | $2.9 \cdot 10^{24}$ | 0.048 | $2.1 \cdot 10^{24}$ | 0.20 | $5.1 \cdot 10^{23}$ | 0.3 | $3.4 \cdot 10^{23}$ | 1.0 | $1.0 \cdot 10^{23}$ |
| 150 | 0.052 | $1.9 \cdot 10^{24}$ | 0.098 | $1.0 \cdot 10^{24}$ | 0.45 | $2.2 \cdot 10^{23}$ | 0.7 | $1.4 \cdot 10^{23}$ | 2.3 | $4.4 \cdot 10^{22}$ |
| 200 | 0.046 | $2.2 \cdot 10^{24}$ | 0.122 | $8.2 \cdot 10^{23}$ | 0.65 | $1.5 \cdot 10^{23}$ | 1.1 | $9.5 \cdot 10^{22}$ | 3.5 | $2.9 \cdot 10^{22}$ |
| 300 | 0.023 | $4.3 \cdot 10^{24}$ | 0.112 | $8.9 \cdot 10^{23}$ | 0.90 | $1.1 \cdot 10^{23}$ | 1.6 | $6.4 \cdot 10^{22}$ | 5.4 | $1.9 \cdot 10^{22}$ |
| 400 | 0.013 | $7.7 \cdot 10^{24}$ | 0.081 | $1.2 \cdot 10^{23}$ | 0.97 | $1.0 \cdot 10^{23}$ | 1.8 | $5.6 \cdot 10^{22}$ | 6.4 | $1.6 \cdot 10^{22}$ |
| 500 | 0.008 | $1.2 \cdot 10^{25}$ | 0.055 | $1.8 \cdot 10^{24}$ | 0.96 | $1.0 \cdot 10^{23}$ | 1.9 | $5.3 \cdot 10^{22}$ | 7.1 | $1.4 \cdot 10^{22}$ |
| 600 | 0.006 | $1.8 \cdot 10^{25}$ | 0.038 | $2.7 \cdot 10^{24}$ | 0.91 | $1.1 \cdot 10^{23}$ | 1.9 | $5.2 \cdot 10^{22}$ | 7.5 | $1.3 \cdot 10^{22}$ |
| 730 | 0.003 | $2.9 \cdot 10^{25}$ | 0.025 | $4.0 \cdot 10^{24}$ | 0.83 | $1.2 \cdot 10^{23}$ | 1.9 | $5.2 \cdot 10^{22}$ | 7.8 | $1.3 \cdot 10^{22}$ |

Table 2: Integrated $\nu_{\mu}CC$ events per kton and 10^{19} p.o.t within the relevant energy interval $N_{\mu,CC}^0$ and integrated beam intensity \mathcal{I}_{pot} , assuming a constant 20% focusing efficiency wrt perfect focusing, needed to obtain $N_e = 5$ events (see text) as a function of the baseline L for various proton energies. The configuration corresponding to the minimum \mathcal{I}_{pot} is shown in bold.

each proton energy there is an optimal baseline L^{opt} , which maximizes the integrated neutrino oscillation probability in the neutrino energy region which corresponds to the largest weighted pion yield at that proton energy.

For a 2.2 GeV proton driver, the optimal baseline L^{opt} is approximately $L^{opt} \approx 150$ km. For a 4.4 GeV proton driver, it is approximately $L^{opt} \approx 200$ km. For 20 GeV, we find $L^{opt} \approx 450$ km. For energies above 50 GeV, the optimal baseline is around 700 km.

For actual baselines smaller than the optimal baseline, $L < L^{opt}$, the neutrino oscillation maximum occurs at lower energy and the yield of corresponding pions for the given proton energy is lower than in the optimal case. Hence, we need a higher intensity to compensate for this effect.

For actual baselines greater than the optimal baseline, $L > L^{opt}$, the neutrino oscillation maximum occurs at higher energy and the yield of corresponding pions for the given proton energy is lower than in the optimal case. Indeed, at some point, the optimal neutrino oscillation energy corresponds to a pion energy, which is kinematically forbidden for the given incident proton energy. Hence, we need again a higher proton intensity to compensate for the kinematical suppression.

At the optimal baselines L_{opt} the power factors are the following:

$$\mathcal{F}_{2.2} \approx 2.2 \times 1.9 \times 10^{24} = 4.2 \times 10^{24} \text{ GeV} \times \text{pot}, \quad (10)$$

$$\mathcal{F}_{4.4} \approx 4.4 \times 8.2 \times 10^{23} = 3.6 \times 10^{24} \text{ GeV} \times \text{pot}, \quad (11)$$

$$\mathcal{F}_{20} \approx 20 \times 1.0 \times 10^{23} = 2.0 \times 10^{24} \text{ GeV} \times \text{pot}, \quad (12)$$

$$\mathcal{F}_{50} \approx 50 \times 5.2 \times 10^{22} = 2.6 \times 10^{24} \text{ GeV} \times \text{pot}, \quad (13)$$

$$\mathcal{F}_{400} \approx 400 \times 1.3 \times 10^{22} = 5.2 \times 10^{24} \text{ GeV} \times \text{pot.} \quad (14)$$

This directly confirms the approximate scaling with \mathcal{F} , apart at the lowest and the highest proton energies. Strictly speaking, a proton energy of 20 GeV appears to be the most economical choice in terms of protons, with a proton economy of about a factor 2 compared to the 2.2 and 400 GeV cases.

Summarizing, the required protons on target for 5 oscillated events at $\Delta m^2 = 3 \times 10^{-3} \text{ eV}^2$ and $\sin^2 2\theta_{13} = 10^{-3}$ in the 2.35 kton mass located *at the optimal baseline* assuming a 20% ideal focusing are $\approx 2 \times 10^{24}$ for 2.2 GeV protons, $\approx 10^{24}$ for 4.4 GeV, $\approx 10^{23}$ for 20 GeV, $\approx 5 \times 10^{22}$ for 50 GeV and $\approx 10^{22}$ for 400 GeV.

5 Results in real focusing

The standard focusing system for all neutrino beams up to now is based on magnetic horns. However, new solutions should be envisaged for low-energy, intense beams. The angular acceptance of the system has to be large (the average transverse momentum of reaction products is of the order of 200-300 MeV, comparable with the total momentum for the shortest baselines), and the amount of material within the secondary beam cone must be as little as possible, both to preserve the flux and to avoid heating/damage at high intensities.

In principle, the focusing system should cancel the transverse momentum of all secondary particles relative to the direction of flight toward the detector and this *independently of their momentum p* . Indeed, this is the definition of the ideal focusing.

In practice, a horn system can be designed to focalize a given signed momentum, i.e. like p . A FODO system focalizes like $|p|$. A series of coils should focalize like 1, i.e. independent of p . Hence, this last solution seems to be attractive in our situation.

We have found with the help of full simulations and tracking of the particles in the focusing system that (1) for the lowest energy configuration, a series of coils does indeed provide a quite optimal focusing and (2) for the higher energy configurations, where the coil focusing becomes impracticable, the traditional horn focusing can be efficiently used.

5.1 Details on coil focusing

One possible solution is to exploit the focusing capabilities of magnetic field gradients, such as the fringe field at the ends of a solenoid, or the decreasing field far from a current loop. The fact that a particle traveling almost parallel to the axis of a solenoid suffers a change of its transverse momentum when traversing the fringe region is not intuitive but can be understood by realizing that any change of the longitudinal component of

an axially symmetric field is associated through Maxwell's divergence equation to a radial component of the field.

The particle motion in axially symmetric fields can be described on the basis of the Busch's theorem, which in turn follows from the conservation of canonical angular momentum. The derivation and applications of this theorem can be found in textbooks (see for instance [18, 19]), here we give a summary to better illustrate our focusing system. Suppose we have a particle having electric charge q and total energy E , moving in a static, non-uniform axially symmetric field, at a distance r from the field axis (z -axis), with an angular velocity $\dot{\phi}$. Busch's theorem states that

$$rp_\phi + \frac{q}{2\pi}\Psi = \text{const} \quad (15)$$

where $p_\phi = \gamma m \dot{\phi}$ is the azimuthal component of the particle momentum, and Ψ is the magnetic flux linked by a circle of radius r centered on the field axis.

If the field can be considered constant within the circle of radius r , we have

$$\Psi = \pi r^2 B_z, \text{ thus } rp_\phi + \frac{q}{2}r^2 B_z = \text{const} \quad (16)$$

If particles are emitted with zero angular velocity by a source located on the axis of an axially symmetric magnetic field, both the angular momentum and Ψ are null, thus $\text{const} = 0$.

When exiting to a region of zero field, according to Busch's theorem the particles will have *zero* angular momentum. This is very appealing remembering that in an uniform (solenoidal) field, all the transverse momentum is azimuthal. However, this is not the case when the field varies, and part of the momentum can also be directed along the radius. The radial motion can also be derived exploiting Busch's theorem, but the practical use is not straightforward.

However, if the variation of the magnetic field is small on the scale of the revolution time, the theorem of adiabatic invariance states that the magnetic flux encircled by the particle trajectory remains a constant of motion. The trajectory radius can be assumed constant over a revolution and given by the usual expression

$$R = \frac{p_T}{qB_z},$$

and from adiabatic invariance follows

$$B_z R^2 \pi = \frac{\pi p_T^2}{q^2 B_z} = \text{const.}$$

Under this condition, all the rotational motion is converted into the longitudinal one, and the particle transverse momentum varies as

$$\frac{p_T^2}{B_z} = \frac{p_{T0}^2}{B_{z0}} \quad (17)$$

where B_{z0} , p_{T0}^2 are the initial magnetic field and transverse momentum.

Since the period of the motion is

$$\tau = \frac{2\pi}{\omega_B} = \frac{2\pi E}{qB_z},$$

the condition of adiabatic motion means that ΔB_z must be small over distances

$$\Delta z = \frac{2\pi E v_{\parallel}}{qB_z} = \frac{2\pi p_{\parallel}}{qB_z}.$$

For a pion having a longitudinal momentum of 1 GeV/c, in B=1 T, Δz is about 20 m. It is thus difficult to focus efficiently high energy particles through fringe fields, while this method can be very effective for low energy ones. It should be stressed that this method applies equally well to positive and negative particles, even though the resulting advantage is not great since the positive component is dominant for low energy beams.

| Baseline L km | 2.2 GeV coil focus | | 4.4 GeV coil focus | | 20 GeV horn focus | | 400 GeV horn focus | |
|--------------------|-----------------------|---------------------------------------|-----------------------|---------------------------------------|----------------------|---------------------------------------|-----------------------|---------------------------------------|
| | $N_{\mu,CC}^0$ | \mathcal{I}_{pot} | $N_{\mu,CC}^0$ | \mathcal{I}_{pot} | $N_{\mu,CC}^0$ | \mathcal{I}_{pot} | $N_{\mu,CC}^0$ | \mathcal{I}_{pot} |
| 100 | 0.022 | $9.1 \cdot 10^{23}$ | 0.036 | $5.6 \cdot 10^{23}$ | 0.10 | $2.1 \cdot 10^{23}$ | 0.2 | $1.0 \cdot 10^{23}$ |
| 150 | 0.025 | $8.0 \cdot 10^{23}$ | 0.053 | $3.8 \cdot 10^{23}$ | 0.21 | $9.5 \cdot 10^{22}$ | 0.6 | $3.1 \cdot 10^{22}$ |
| 200 | 0.019 | $1.0 \cdot 10^{24}$ | 0.053 | $3.8 \cdot 10^{23}$ | 0.31 | $6.5 \cdot 10^{22}$ | 1.4 | $1.5 \cdot 10^{22}$ |
| 300 | 0.009 | $2.2 \cdot 10^{24}$ | 0.027 | $7.5 \cdot 10^{23}$ | 0.38 | $5.3 \cdot 10^{22}$ | 2.0 | $9.8 \cdot 10^{21}$ |
| 400 | 0.005 | $4.0 \cdot 10^{24}$ | 0.015 | $1.3 \cdot 10^{24}$ | 0.39 | $5.2 \cdot 10^{22}$ | 2.5 | $8.0 \cdot 10^{21}$ |
| 500 | 0.003 | $6.4 \cdot 10^{24}$ | 0.010 | $2.1 \cdot 10^{24}$ | 0.38 | $5.2 \cdot 10^{22}$ | 3.0 | $6.8 \cdot 10^{21}$ |
| 600 | 0.002 | $9.8 \cdot 10^{24}$ | 0.006 | $3.1 \cdot 10^{24}$ | 0.38 | $5.2 \cdot 10^{22}$ | 3.7 | $5.4 \cdot 10^{21}$ |
| 730 | 0.001 | $1.6 \cdot 10^{25}$ | 0.004 | $4.9 \cdot 10^{24}$ | 0.35 | $5.8 \cdot 10^{22}$ | 3.8 | $5.2 \cdot 10^{21}$ |

Table 3: Same as Table 2 with the focusing system included in the simulations. The configuration corresponding to the minimum \mathcal{I}_{pot} is shown in bold. It is computed in order to obtain a number of oscillated events $N_e = 5$ (see text) for the various baselines L and proton energies.

5.2 Results on horn and coil focusing

We report in Table 3 our results with full detailed simulations of the focusing systems for 2.2 GeV 4.4 GeV, 20 GeV and 400 GeV proton energies.

The coil method has been applied here to the 2.2 and 4.4 GeV proton beams, where the produced pions have small energies (only positive mesons have been considered in Table 3). The target has been assumed to be a short (30 cm) mercury target, like

in the SPL[16] proposal. The non-uniform magnetic field has been obtained with ten circular loops, having a radius of 1 m, positioned from 0 to 14 meters from the target, carrying decreasing currents to give a field from 20 T to zero. Examples of particle orbits and the central magnetic field intensity are shown in Figure 4. The effect on the transverse momentum distribution can be appreciated from Figure 5, where positive pions emitted from the target within 1 radian have been considered. The decay tunnel is 150 m long.

For higher energy neutrino beams of 20 GeV and 400 GeV, the traditional two-horns system has been used. The calculations presented here refer to a first horn to focus 2 GeV/c particles, followed by a reflector to focus 3 GeV/c. The horn is placed around a graphite target, has a length of 4 meters and a current of 300 kA. The reflector starts at 6 m from the target, is 4 m long with a current of 150 kA. Examples of particle trajectories can be seen in Figure 6, and the effect on the transverse momentum in the case of a 20 GeV primary beam is shown in Figure 7. The decay tunnel is 350 m long.

In the total energy range (0-2.5 GeV), the resulting focusing efficiency varies in between 0.5 and 0.2. This motivated our choice in Section 4, when comparing all possible beam/distance options, where a common energy-independent 20% focusing efficiency had been assumed. In reality, the focusing profile is not energy independent, and the real situation can be better than this, as can be derived from the comparison of Tables 2 and 3. This effect is also visible in Figure 8.

Summarizing, the required protons on target for 5 oscillated events at $\Delta m^2 = 3 \times 10^{-3} \text{ eV}^2$ and $\sin^2 2\theta_{13} = 10^{-3}$ in the 2.35 kton mass located *at the optimal baseline* assuming optimized realistic focusing are $\approx 1 \times 10^{24}$ for 2.2 GeV protons, $\approx 4 \times 10^{23}$ for 4.4 GeV, $\approx 5 \times 10^{22}$ for 20 GeV and $\approx 5 \times 10^{21}$ for 400 GeV.

The cautious reader can wonder why we have apparently been “conservative” in assuming a 20% efficiency for the ideal focusing. The point here is that in the ideal case we assume a constant efficiency over the whole meson energy range, while in the real focusing case one effectively reaches a situation where a part of the meson energy range is focalized with an efficiency better than 20% while other parts have lower efficiencies. We have of course optimized focusing for the energy relevant to the oscillation. It would however be incorrect to assume that this higher efficiency is constant over the full energy range.

6 A superbeam to Gran Sasso (BNGS²) ?

6.1 Finding the location for the source

As a working hypothesis, we take for granted the existence of LNGS as an underground laboratory that can host large neutrino detectors. In particular, we have assumed for

²BNGS stands for “Better Neutrinos to GS”.

| Laboratory | Lat. | Long. | Baseline to LNGS (km) | Angle | Inclination |
|--------------------|-------|-------|--------------------------|-------|-------------|
| Casaccia (ENEA) | 42° | 12.2° | 120 | 63° | 0.54° |
| Napoli (ENEA) | 40.8° | 14.3° | 200 | 145° | 0.9° |
| Aquilone (ENEA) | 41.7° | 15.9° | 217 | 166° | 1.° |
| Brasimone (ENEA) | 44.2° | 11.1° | 270 | 8° | 1.2° |
| Legnaro (INFN) | 45.4° | 12.0° | 344 | 34° | 1.5° |
| Trisaia (ENEA) | 40.3° | 16.8° | 368 | 173° | 1.65° |
| Pavia (INFN,Univ.) | 45.2° | 9.2° | 465 | 5.7° | 2.1° |
| Ispra (ENEA,CCR) | 45.8° | 8.6° | 536 | 8.5° | 2.4° |
| Catania (INFN) | 37.5° | 15.1° | 570 | 140° | 1.5° |
| CERN | 46.1° | 6.0° | 732 | 0.0° | 3.22° |

Table 4: List of existing laboratories with interesting baselines to the LNGS Gran Sasso laboratory. Angle is the space angle relative to the orientation of the LNGS Halls. Inclination is the incoming neutrino angle relative to the horizontal plane at LNGS.

this study the existence of ICARUS with 2.35 kton fiducial mass.

If we take the location of the detector as fixed, the baseline L is determined by the location of the neutrino source. We have investigated various potential locations within Italy where large ENEA³ or INFN infrastructures are already existing, as shown in Table 4. In these locations, the required conditions to host a high intensity proton driver could be met and the machine would find other applications in addition to neutrino physics.

In Table 4, the column called “angle” describes the space angle relative to the orientation of the LNGS Halls. Inclination is the incoming neutrino angle relative to the horizontal plane at LNGS. We note that due to the fortunate orientation of the LNGS Halls according to the geographical axis of the Italian peninsula, it is possible to find various laboratories within the orientation of the LNGS Halls.

Indeed, ENEA Aquilone, ENEA Brasimone, ENEA Trisaia, INFN Pavia and ENEA Ispra appear with an angle less than 15° with respect to the LNGS Hall direction. This is an advantage for the acceptance of higher energy events given the natural longitudinal orientation of the detectors. On the other hand, in the case of ENEA Casaccia situated near Rome, the angle is 63°. However, for the shortest baseline, we expect the relevant neutrinos to have an energy similar to that of most atmospheric neutrinos, so that we can argue that the acceptance will not be a problem given the isotropical nature of a detector like ICARUS.

³ENEA stands for “Ente per le Nuove Tecnologie, l’Energia e l’Ambiente”.

| E_p GeV | Focus | Decay tunnel length (m) | ν_μ flux ν/cm^2 | ν_e flux ν/cm^2 | 10^{23} p.o.t. | | $\langle E_\nu \rangle$, CC | | ν_e/ν_μ CC |
|--------------|-------|----------------------------|-------------------------------------|-----------------------------------|-----------------------------|------------|------------------------------|----------------|-----------------------|
| | | | | | ν_μ CC events/kton | ν_e CC | ν_μ GeV | ν_e GeV | |
| 2.2 | p.f. | 150 | 1.6×10^{-11} | 8.0×10^{-13} | 285 | 4.9 | 0.47 | 0.53 | 1.7% |
| 2.2 | coil | 150 | 9.5×10^{-12} | 1.2×10^{-13} | 109 | 2.2 | 0.41 | 0.56 | 2.1% |
| 4.4 | p.f. | 150 | 5.7×10^{-11} | 1.6×10^{-12} | 1900 | 28 | 0.77 | 0.96 | 1.5% |
| 4.4 | coil | 150 | 2.0×10^{-11} | 9.5×10^{-13} | 340 | 5.6 | 0.56 | 0.6 | 1.6% |
| 20 | p.f. | 350 | 1.1×10^{-9} | 2.3×10^{-11} | 6.6×10^4 | 800 | 1.6 | 1.4 | 1.3% |
| 20 | horn | 350 | 4.4×10^{-10} | 7.3×10^{-12} | 2.6×10^4 | 310 | 1.6 | 1.3 | 1.2% |

Table 5: Neutrino beam parameters for a 270 km baseline experiment. All quantities are calculated for $0 < E_\nu < 2.5$ GeV

6.2 The medium baselines ($120 < L < 470$ km)

We study the cases ENEA Casaccia ($L = 120$ km), ENEA Brasimone ($L = 270$ km) and INFN Pavia ($L = 465$ km). At these distances, the neutrino energy range relevant for $\nu_\mu \rightarrow \nu_e$ search is 0.1-1.0 GeV. We assume 2.2, 4.4 and 20 GeV proton energies. Expected neutrino fluxes and rates, obtained assuming ideal (p.f.) and real (coil or horn) focusing systems, are reported in Table 5. The figures are normalized to the baseline $L = 270$ km and for $0 \leq E_\nu \leq 2.5$ GeV. Other baselines can be rescaled accordingly. With real focusing, we find about 100(10) $\nu_\mu(\bar{\nu}_\mu)$ CC events/kton per 10^{23} pots for 2.2 GeV protons, about 340(40) $\nu_\mu(\bar{\nu}_\mu)$ CC events/kton for 4.4 GeV protons and about 26000(250) $\nu_\mu(\bar{\nu}_\mu)$ CC events/kton for 20 GeV protons. Intrinsic $\nu_e(\bar{\nu}_e)$ beam contaminations are in the range from 1% to 2% with respect to $\nu_\mu(\bar{\nu}_\mu)$.

The 2.2 and 4.4 GeV proton energies are the closest to the optimal energies and only these two cases are considered in the following. We will consider 20 GeV in section 6.3 in the context of the CERN-LNGS baseline.

To appreciate the matching between the neutrino beams and the oscillation probability, we show in Figures 9 and 10 the charged current event rate at 120 km as a function of the neutrino energy. The dotted lines correspond to the oscillation probability (arb. norm.) for a $\Delta m^2 = 3 \times 10^{-3}$ eV².

Clearly, these neutrino beams offer optimal condition to study ν_μ *disappearance*. Indeed, the maximum of the oscillation is very well covered by the neutrino beam and hence it is quite obvious that a very precise determination of the main oscillation parameters will be accomplished. We here do not consider this any further.

We, however, concentrate instead on the ν_e *appearance* measurement. Since we are in the presence of intrinsic ν_e background from the beam at the level of 1%-2% of the ν_μ component, we can improve our sensitivity by studying the energy spectrum of the ν_e charged current events. This method is more sensitive than simple event counting.

In order to estimate the sensitivity, we adopt our standard fitting procedure of the various reconstructed event classes (See Ref. [20]). We assume that the neutrino and antineutrino interactions cannot be distinguished on an event-by-event basis, and hence add the ν_e and $\bar{\nu}_e$ contributions from the beam. Similarly, the oscillated spectrum is calculated by summing both $\nu_\mu \rightarrow \nu_e$ and $\bar{\nu}_\mu \rightarrow \bar{\nu}_e$ oscillations, assuming the same oscillation probability for neutrino and antineutrinos.

In the present study, we considered only the energy distribution of electron events and computed the χ^2 as a function of the $\sin^2 2\theta_{13}$ mixing angle, scanning in Δm^2 . The 90% C.L. sensitivity region is defined by the condition $\chi^2 > \chi_{min}^2 + 4.6$, defined by the condition that the actually observed events in the experiment coincide with the expected background. In an actual experiment, a simultaneous fit of the muon disappearance and electron appearance spectra will constrain the Δm^2 , $\sin^2 \theta_{23}$ parameters and in case of negative result will limit the $\sin^2 2\theta_{13}$ within the allowed Δm^2 region.

The results of the Δm^2 scans are shown in Figure 11 for 2.2 GeV and Figure 12 for 4.4 GeV proton energy for the three assumed baselines. The curves correspond to 5 years running with 2×10^{23} pots/year equivalent to a continuous proton current of 1 mA and a fiducial mass of 2.35 kton. The assumed protons on target is compatible with an accelerator with performances similar to those of the planned CERN-SPL[16].

The expected sensitivities represent a great improvement to the CHOOZ limit[10] which gives for $\Delta m^2 = 2.5 \times 10^{-3} \text{ eV}^2$,

$$(\sin^2 2\theta_{13})_{CHOOZ} < 0.14 \quad \text{or} \quad \theta_{13} < 11^\circ \quad (18)$$

Indeed, we find for 2.2 GeV protons:

$$(\sin^2 2\theta_{13})_{BNGS,120km} < 0.006 \quad \text{or} \quad \theta_{13} < 2.2^\circ \quad (19)$$

$$(\sin^2 2\theta_{13})_{BNGS,270km} < 0.015 \quad \text{or} \quad \theta_{13} < 3.4^\circ \quad (20)$$

$$(\sin^2 2\theta_{13})_{BNGS,465km} < 0.03 \quad \text{or} \quad \theta_{13} < 5^\circ \quad (21)$$

and for 4.4 GeV protons:

$$(\sin^2 2\theta_{13})_{BNGS,120km} < 0.0035 \quad \text{or} \quad \theta_{13} < 1.7^\circ \quad (22)$$

$$(\sin^2 2\theta_{13})_{BNGS,270km} < 0.006 \quad \text{or} \quad \theta_{13} < 2.2^\circ \quad (23)$$

$$(\sin^2 2\theta_{13})_{BNGS,465km} < 0.02 \quad \text{or} \quad \theta_{13} < 4^\circ \quad (24)$$

For comparison, the JHF proposal with the OAB beam gives similar results[11]

$$(\sin^2 2\theta_{13})_{JHF,OAB} < 0.006 \quad \text{or} \quad \theta_{13} < 2.2^\circ. \quad (25)$$

6.3 The CERN-GS baseline

The baseline between CERN and GS is 730 km. At this distance, the neutrino energy range relevant for $\nu_\mu \rightarrow \nu_e$ search is 0.3-2.5 GeV.

The present CNGS design[8] is optimized for ν_τ appearance, thus for a relatively high-energy neutrino beam. The 400 GeV/c SPS beam will deliver $4.5 \cdot 10^{19}$ protons per year on a graphite target, made of spaced rods to reduce the re-interaction rate. The two magnetic horns (horn and reflector) are tuned to focus 35 and 50 GeV/c mesons, with an acceptance of the order of 30 mrad. The decay tunnel length is 1 km. With the standard CNGS parameters, the low-energy neutrino flux is low, as can be seen from the entries flagged by \dagger in Table 6.

In Ref. [12], we have studied a L.E. optimization of the 400 GeV protons of the CNGS in order to improve the sensitivity to θ_{13} . This yielded an improvement of a factor 5 in flux at low energy compared to the τ optimization.

Here, we study the 20 GeV proton energy (we call this the PS++) and compare it to 400 GeV. Expected neutrino fluxes and rates obtained with real focusing systems are reported in Table 6.

The results of the $\Delta m^2 - \sin^2 2\theta_{13}$ sensitivity scans are shown in Figure 14. The curves correspond to 5 years running with 2×10^{21} or 2×10^{22} pots/year and a fiducial mass of 2.35 kton.

We find for $\Delta m^2 = 2.5 \times 10^{-3} \text{ eV}^2$:

$$(\sin^2 2\theta_{13})_{PS++, 2 \times 10^{21} \text{ pot/year}} < 0.016 \quad \text{or} \quad \theta_{13} < 3.6^\circ \quad (26)$$

$$(\sin^2 2\theta_{13})_{PS++, 2 \times 10^{22} \text{ pot/year}} < 0.005 \quad \text{or} \quad \theta_{13} < 2^\circ \quad (27)$$

Clearly, a strongly intensity-upgraded CERN PS booster would provide very interesting possibilities for the oscillation searches over the CERN-GS baseline.

| E_p GeV | focus | Decay tunnel length (m) | ν_μ flux ν/cm^2 | ν_e flux ν/cm^2 | 10^{19} p.o.t. | | $\langle E_\nu \rangle$, CC | | ν_e/ν_μ CC |
|--------------|----------------|----------------------------|-------------------------------------|-----------------------------------|------------------|----------------------|------------------------------|---------|-----------------------|
| | | | | | ν_μ CC | ν_e CC | ν_μ | ν_e | |
| 20 | p.f. | 150 | 9.8×10^{-15} | 1.6×10^{-16} | 0.56 | 4.1×10^{-3} | 1.5 | 1.26 | 0.7% |
| 20 | p.f. | 350 | 1.5×10^{-14} | 3.1×10^{-16} | 0.9 | 0.011 | 1.6 | 1.4 | 1.3% |
| 20 | horn | 350 | 6.1×10^{-15} | 1.0×10^{-16} | 0.36 | 4.2×10^{-3} | 1.6 | 1.3 | 1.2% |
| 400 | p.f. | 350 | 1.3×10^{-13} | 2.6×10^{-15} | 9.0 | 0.12 | 1.8 | 1.8 | 1.3% |
| 400 | horn | 350 | 1.0×10^{-15} | 9.0×10^{-16} | 4.5 | 4.2×10^{-2} | 1.8 | 1.4 | 0.9% |
| 400 | p.f. \dagger | CNGS | 1.6×10^{-14} | 3.2×10^{-16} | 1.8 | 2.2×10^{-2} | 2.1 | 1.7 | 1.2% |
| 400 | τ^\dagger | CNGS | 1×10^{-14} | 9.4×10^{-17} | 0.9 | 8.7×10^{-3} | 1.8 | 1.8 | 0.9% |

Table 6: Neutrino beam parameters for the CNGS baseline, with $E_\nu < 2.5$ GeV. The \dagger cases correspond to the *present CNGS design* for target, acceptance and focusing system.

7 The intrinsic ν_e background

As well known, the intrinsic electron (anti)neutrinos in the beam are produced either in the decay of muons coming from kaons or pions via the chain

$$\pi^+/K^+ \rightarrow \mu^+ + \nu_\mu, \quad \mu^+ \rightarrow \nu_e + e^+ + \bar{\nu}_\mu,$$

or directly in the three-body K_{e3} kaon decays.

When looking for $\nu_\mu \rightarrow \nu_e$ oscillations, this contamination will eventually be the limiting factor. It is therefore essential to understand its level and it is also worth understanding if the beam design can be optimized to minimize this background.

Rather than the ν_e/ν_μ ratio, we decide to consider the ratio $\nu_\mu/\sqrt{\nu_e}$ in order to better estimate the effect of the background on the $\nu_\mu \rightarrow \nu_e$ oscillation sensitivity.

Which source of ν_e is relevant to our study?

Due to the large difference between the π and μ decay lengths, the electron neutrino background depends on the length of the decay tunnel l . This dependence should be more evident for low beam energies.

Kaon production strongly depends on the proton energy, as shown in Figure 15, where a threshold effect is clearly visible. For the lowest proton energies, 2.2 and 4.4 GeV, the fraction of kaon relative to pions is a few per mille. Above 20 GeV, it is on the order of a little less than 10%.

At low ν_e energies, the production is shared by kaon and muon decays, while kaon decays alone are responsible for the high energy tail. For low proton beam energies, kaon production is much lower and practically all the intrinsic electron contamination comes from muon decays.

A first order estimate of the effect of the decay tunnel length l on the muon-induced background can be derived assuming forward decay at each step, and counting for each neutrino energy the fraction of parent particles that decay within a path l . The fraction D_π of π decayed after a length l is simply given by

$$D_\pi = (1 - e^{-\frac{l}{\lambda_\pi}}) \tag{28}$$

Muons have to be generated by a pion first, thus

$$\begin{aligned} D_\mu &= \int_0^l \lambda'_\pi e^{-\frac{y}{\lambda'_\pi}} \cdot \left(1 - e^{-\frac{l-y}{\lambda'_\mu}}\right) dy \\ &= 1 - \frac{1}{\lambda'_\mu - \lambda'_\pi} \left(\lambda'_\mu e^{-\frac{l}{\lambda'_\mu}} - \lambda'_\pi e^{-\frac{l}{\lambda'_\pi}}\right) \end{aligned} \tag{29}$$

The decay lengths $\lambda'_\pi, \lambda'_\mu$ depend on the energy of the meson. We can fix a neutrino energy E_ν , the same for ν_μ and ν_e . For ν_μ production, we can then assume $p_\pi =$

$E_\nu/0.43$. For the ν_e produced in the decay of a muon, there is no fixed relation, but we can take the average of the ν_e energy in the muon rest frame, getting $p_\mu \approx E_\nu/0.6$. The grand-parent pion had therefore a momentum equal to $p'_\pi \approx p_\mu \approx E_\nu/0.6$.

With these approximations, D_π and D_μ can be expressed as a function of l/E_ν . In these units, one π decay length corresponds to $l/E_\nu = 130 \text{ m/GeV}$.

It is a priori obvious that short decay tunnels reduce the relative probability of muon production and decay. However, the pion decay yield is also affected.

To study the background from muons, we consider the statistically significant ratio $\pi \text{decays}/\sqrt{\mu \text{decays}}$ as the correct estimator for $\nu_\mu/\sqrt{\nu_e}$ as a function of the decay tunnel length. This ratio is shown in Figure 16, where the assumption of a fixed ν_e energy in μ decay has been relieved: the hatched band corresponds to 20%-80% of the maximum ν_e energy in the μ rest frame.

We find that the ratio does not show dramatic variations between 0 and 4 pion decay lengths. We therefore conclude that *not much is to be gained by reducing the length of the decay tunnel*.

We have verified these results directly by the full simulation of the neutrino beams for various decay tunnel lengths. Answers are reported in Table 7 for various proton energies and decay tunnel lengths. The 6th column shows the expected ν_e contamination relative to the ν_μ and the last column lists the statistically relevant ratio $\nu_\mu/\sqrt{\nu_e}$. For the 2.2 GeV proton energy, the ratio ν_e/ν_μ varies from 0.3% for $l = 20 \text{ m}$ up to 1.7% for $l = 150 \text{ m}$, but this happens at a high cost of genuine ν_μ 's. The statistically relevant ratio $\nu_\mu/\sqrt{\nu_e}$ varies from 0.67 for $l = 20 \text{ m}$ down to 0.47 for $l = 150 \text{ m}$. This is a modest loss. We also stress that the naive \sqrt{N} scaling is not adequate for an appearance experiment where we are looking for few events and hence we conclude that genuine ν_μ rate is more important than a slightly better ν_e/ν_μ ratio.

Remains the issue of the proton energy. Naively, one would expect that the higher the proton energy, the higher is the background. We find however that the intrinsic electron neutrino background does *not* strongly depend on the proton energy.

This was verified directly for various proton energies and baselines. Results of the calculation are shown in Table 8, all normalized to 10^{19} pots. We observe that (1) for the shortest baselines, the ratio ν_e/ν_μ is increasing dramatically with proton energy. Accordingly, (2) the ratio $\nu_\mu/\sqrt{\nu_e}$ decreases. However, we must rescale this ratio to take into account the approximate scaling of the number of events with the proton energy. Since we expect

$$\frac{\nu_\mu}{\sqrt{\nu_e}} \propto \frac{E_p}{\sqrt{E_p}} \propto \sqrt{E_p} \quad (30)$$

we consider the rescaled ratio $\nu_\mu/\sqrt{\nu_e \cdot E_p}$ in the last columns of the Table 8. These are also plotted in Figure 17 as a function of the baseline L . Numerically, we find that *the rescaled ratios $\nu_\mu/\sqrt{\nu_e \cdot E_p}$ are almost the identical at the optimal baselines of each proton energy*, so not much is too be gained by varying the proton energy.

Summarizing, we find that the electron neutrino background in the relevant region is not dependent on the proton energy and only determined by the decay tunnel length, but that its optimisation is very limited. For the maximum neutrino muon flux, it is at the level of the 1% for any of the considered setups.

| E_p GeV | Focus | Decay tunnel length, m | ν_μ ev/kton/ 10^{19} | ν_e p.o.t. | ν_e/ν_μ | $\nu_\mu/\sqrt{\nu_e}$ |
|--------------|-------|---------------------------|---------------------------------|----------------------|-----------------|------------------------|
| | | | L=730 km | | | |
| 2.2 | p.f. | 150 | 3.9×10^{-3} | 6.7×10^{-5} | 1.7% | 0.47 |
| 2.2 | p.f. | 50 | 2.5×10^{-3} | 2.1×10^{-5} | 0.84% | 0.55 |
| 2.2 | p.f. | 20 | 1.2×10^{-3} | 3.2×10^{-6} | 0.27% | 0.67 |
| 2.2 | coil | 150 | 1.5×10^{-3} | 3.1×10^{-5} | 2.1% | 0.3 |
| 4.4 | p.f. | 150 | 2.6×10^{-2} | 3.9×10^{-4} | 1.5% | 1.3 |
| 4.4 | coil | 150 | 4.6×10^{-3} | 7.6×10^{-5} | 1.6% | 0.53 |
| 20 | p.f. | 150 | 0.56 | 4.1×10^{-3} | 0.7% | 8.7 |
| 20 | p.f. | 350 | 0.9 | 0.011 | 1.3% | 8.6 |
| 20 | horn | 350 | 0.36 | 4.2×10^{-3} | 1.2% | 5.6 |
| 400 | p.f. | 350 | 9.0 | 0.12 | 1.3% | 26.0 |
| 400 | horn | 350 | 4.5 | 4.2×10^{-2} | 0.9% | 22.0 |

Table 7: Electron neutrino intrinsic background within $E_\nu < 2.5$ GeV for various proton energies and beam optics configurations. For ease of comparison, rates are normalized to a baseline L=730 km.

8 Summary and Conclusions

In this document, we have performed a two-dimensional scan, varying the beam energy and baseline parameters to optimize the conditions for the investigation of θ_{13} driven neutrino oscillations in the whole Superkamiokande allowed Δm^2 range. We find that:

- The optimal baselines for θ_{13} searches are in the range 100-700 km for proton energies varying from 2.2 to 400 GeV.
- The needed beam intensity scales approximately with the inverse of the beam energy.
- In terms of proton economics, the optimum beam energy is around 20 GeV, but lower beam energies are appealing for the shortest baselines.

Realistic focusing system for low and medium baselines have also been studied. In this case:

| L Km | 2.2 GeV coil focus | | | 4.4 GeV coil focus | | | 20 GeV horn focus | | | 400 GeV horn focus | | |
|---------|------------------------------|--------------------------------|--|------------------------------|--------------------------------|--|------------------------------|--------------------------------|--|------------------------------|--------------------------------|--|
| | $\frac{\nu_e}{\nu_\mu} (\%)$ | $\frac{\nu_\mu}{\sqrt{\nu_e}}$ | $\frac{\nu_\mu}{\sqrt{\nu_e \cdot E_p}}$ | $\frac{\nu_e}{\nu_\mu} (\%)$ | $\frac{\nu_\mu}{\sqrt{\nu_e}}$ | $\frac{\nu_\mu}{\sqrt{\nu_e \cdot E_p}}$ | $\frac{\nu_e}{\nu_\mu} (\%)$ | $\frac{\nu_\mu}{\sqrt{\nu_e}}$ | $\frac{\nu_\mu}{\sqrt{\nu_e \cdot E_p}}$ | $\frac{\nu_e}{\nu_\mu} (\%)$ | $\frac{\nu_\mu}{\sqrt{\nu_e}}$ | $\frac{\nu_\mu}{\sqrt{\nu_e \cdot E_p}}$ |
| 100 | 1.6 | 1.2 | 0.79 | 1.6 | 1.5 | 0.72 | 5.9 | 1.3 | 0.28 | 25.7 | 0.9 | 0.05 |
| 150 | 1.4 | 1.3 | 0.91 | 1.2 | 2.1 | 1.00 | 4.1 | 2.3 | 0.51 | 13.5 | 2.2 | 0.11 |
| 200 | 1.4 | 1.2 | 0.79 | 1.1 | 2.2 | 1.06 | 3.2 | 3.1 | 0.69 | 7.6 | 4.1 | 0.20 |
| 300 | 1.8 | 0.7 | 0.48 | 1.4 | 1.4 | 0.66 | 2.0 | 4.3 | 0.97 | 3.3 | 7.8 | 0.39 |
| 400 | 1.8 | 0.5 | 0.35 | 1.6 | 1.0 | 0.46 | 1.6 | 4.9 | 1.08 | 2.1 | 10.7 | 0.54 |
| 500 | 1.9 | 0.4 | 0.27 | 1.6 | 0.8 | 0.36 | 1.4 | 5.2 | 1.16 | 1.6 | 13.7 | 0.68 |
| 600 | 2.0 | 0.3 | 0.22 | 1.6 | 0.6 | 0.30 | 1.2 | 5.6 | 1.24 | 1.2 | 17.7 | 0.89 |
| 730 | 2.1 | 0.2 | 0.16 | 1.7 | 0.5 | 0.24 | 1.1 | 5.6 | 1.25 | 1.0 | 19.5 | 0.97 |

Table 8: Relationships between muon neutrino CC events and electron neutrino CC events, for 10^{19} pots. Event spectra have been integrated over the energy range of interest at each baseline L .

- Focusing efficiencies of 30-50% can be achieved in the energy range of interest.

The whole procedure is detector and accelerator independent. Nevertheless, to give a first estimate of the needed beam intensities, the ICARUS detector has been assumed as a reference.

We can draw the following observations:

- a 2.2 GeV or 4.4 GeV high-intensity proton machine (i.e. à la CERN-SPL) is well matched to a baseline in the range 100-300 km. It is not matched to a baseline of 730 km (i.e. CERN-LNGS).
- a 20 GeV machine is best matched to a baseline of 730 km (i.e. CERN-LNGS). However, an integrated intensity in the range of 10^{23} pots are required, which is about two orders of magnitude higher than the intensity deliverable by the current CERN-PS in a reasonable amount of time.
- a 400 GeV energy is reasonably matched to a baseline of 730 km (i.e. CERN-LNGS). For the 400 GeV, the required intensity is in the range of 10^{22} pots, which is about one order of magnitude higher than the intensity deliverable by the current CERN-SPS in a reasonable amount of time.

Finally, we stress that the present study is essentially a theoretical one. All the “real” work has still to be accomplished in order for one of these options to become reality.

References

- [1] Y. Fukuda *et al.* (Kamiokande Collaboration), *Phys. Lett. B* **335**, 237 (1994).
- [2] Y. Fukuda *et al.* [Super-Kamiokande Collaboration], *Phys. Rev. Lett.* **81**, 1562 (1998) [arXiv:hep-ex/9807003].
- [3] B. Pontecorvo, *J. Expt. Theor. Phys.* **33**, 549 (1957) [*Sov. Phys. JETP* **6**, 429 (1958)]; B. Pontecorvo, *J. Expt. Theor. Phys.* **34**, 247 (1958) [*Sov. Phys. JETP* **7**, 172 (1958)]; Z. Maki, M. Nakagawa and S. Sakata, *Prog. Theor. Phys.* **28** (1962) 870; B. Pontecorvo, *J. Expt. Theor. Phys.* **53** (1967) 1717; V. Gribov and B. Pontecorvo, *Phys. Lett. B* **28**, 493 (1969).
- [4] “E362 Proposal for a long baseline neutrino oscillation experiment, using KEK-PS and Super-Kamiokande”, February 1995.
H. W. Sobel, proceedings of Eighth International Workshop on Neutrino Telescopes, Venice 1999, vol 1 pg 351.
- [5] E. Ables *et al.* [MINOS Collaboration], “P-875: A Long baseline neutrino oscillation experiment at Fermilab,” FERMILAB-PROPOSAL-P-875.
The MINOS detectors Technical Design Report, NuMI-L-337, October 1998.
- [6] ICARUS Collab., “ICARUS-II. A Second-Generation Proton Decay Experiment and Neutrino Observatory at the Gran Sasso Laboratory”, Proposal Vol. I & II, LNGS-94/99, 1994. ICARUS Collab. “A first 600 ton ICARUS Detector Installed at the Gran Sasso Laboratory”, Addendum to proposal, LNGS-95/10 (1995). F. Arneodo *et al.* [ICARUS Collaboration], “Cloning of T600 modules to reach the design sensitive mass”, LNGS-EXP 13/89 add. 2/01, Nov. 2001 and references therein. Available at <http://www.cern.ch/icarus>.
- [7] K. Kodama *et al.* [OPERA Collaboration], “OPERA: a long baseline ν_τ appearance experiment in the CNGS beam from CERN to Gran Sasso”, CERN/SPSC 99-20 SPSC/M635 LNGS-LOI 19/99.
- [8] G. Acquistapace *et al.*, “The CERN neutrino beam to Gran Sasso (NGS)”, Conceptual Technical Design, CERN 98-02 and INFN/AE-98/05 (1998).
- [9] R. Baldy, *et al.* “The CERN neutrino beam to Gran Sasso (NGS)”, Addendum to report CERN 98-02, INFN/AE-98/05, CERN SL-99-034 DI and INFN/AE-99/05 (1999).
- [10] M. Apollonio *et al.* (CHOOZ collaboration), *Phys. Lett.*, B466 (1999) ,415
- [11] Y. Itow *et al.*, “The JHF-Kamioka neutrino project”, KEK report 2001-4, hep-ex/0106019.

- [12] A. Rubbia and P. Sala, “A low-energy optimization of the CERN-NGS neutrino beam for a theta(13) driven neutrino oscillation search,” arXiv:hep-ph/0207084.
- [13] A. Fassò, A. Ferrari, J. Ranft and P.R. Sala, “FLUKA: Status and Perspectives for Hadronic Applications” , Proc. of the Monte Carlo 2000 Conference, Lisbon, 23-26 October 2000, A. Kling et al. eds. ,(Springer, Berlin, 2001)
- [14] A. Fassò, A. Ferrari, J. Ranft and P.R. Sala, “Electron-photon transport in FLUKA: status”, Proc. of the Monte Carlo 2000 Conference, Lisbon, 23-26 October 2000, A. Kling et al. eds. ,(Springer, Berlin, 2001).
- [15] D. Harris, “Comparison of Different Detectors with same Beam”, presented at NNN02, CERN 16-18 January 2002. Available at <http://www.cern.ch/muonstoragerings/NuWorkshop02>.
- [16] B. Autin et al. (the SPL study group), “ Conceptual design of the SPL, a high-power superconducting H⁻ Linac at CERN”, CERN 2000-012 (2000).
- [17] M. Shiozawa, XXth International Conference on Neutrino Physics and Astrophysics, Neutrino 2002, May 2002 (Germany).
- [18] M. Reiser, “Theory and Design of Charged Particle Beams”, (John Wiley & Sons Inc, New York, 1994).
- [19] J.D. Jackson, “Classical Electrodynamics”, third edition, (John Wiley & Sons Inc., New York, 1998).
- [20] A. Bueno, M. Campanelli and A. Rubbia, Nucl. Phys. B **589**, 577 (2000) [arXiv:hep-ph/0005007].

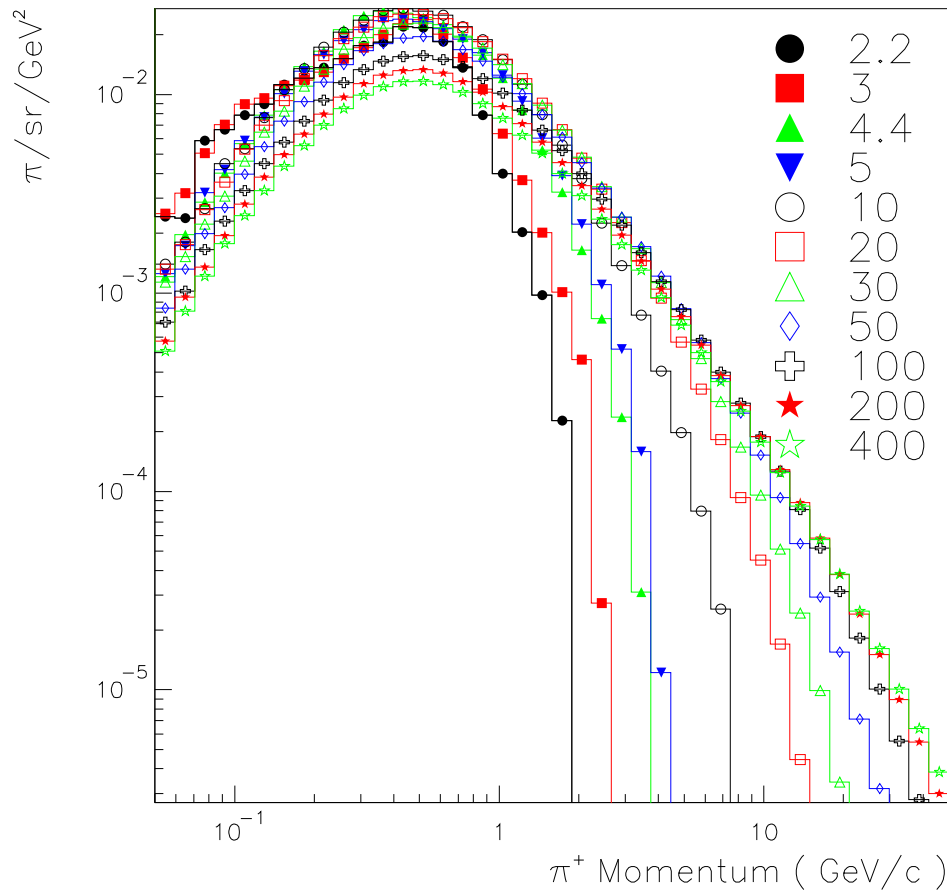


Figure 1: Normalized pion production rate Y_π/E_p for various incident proton energies E_p as estimated with FLUKA.

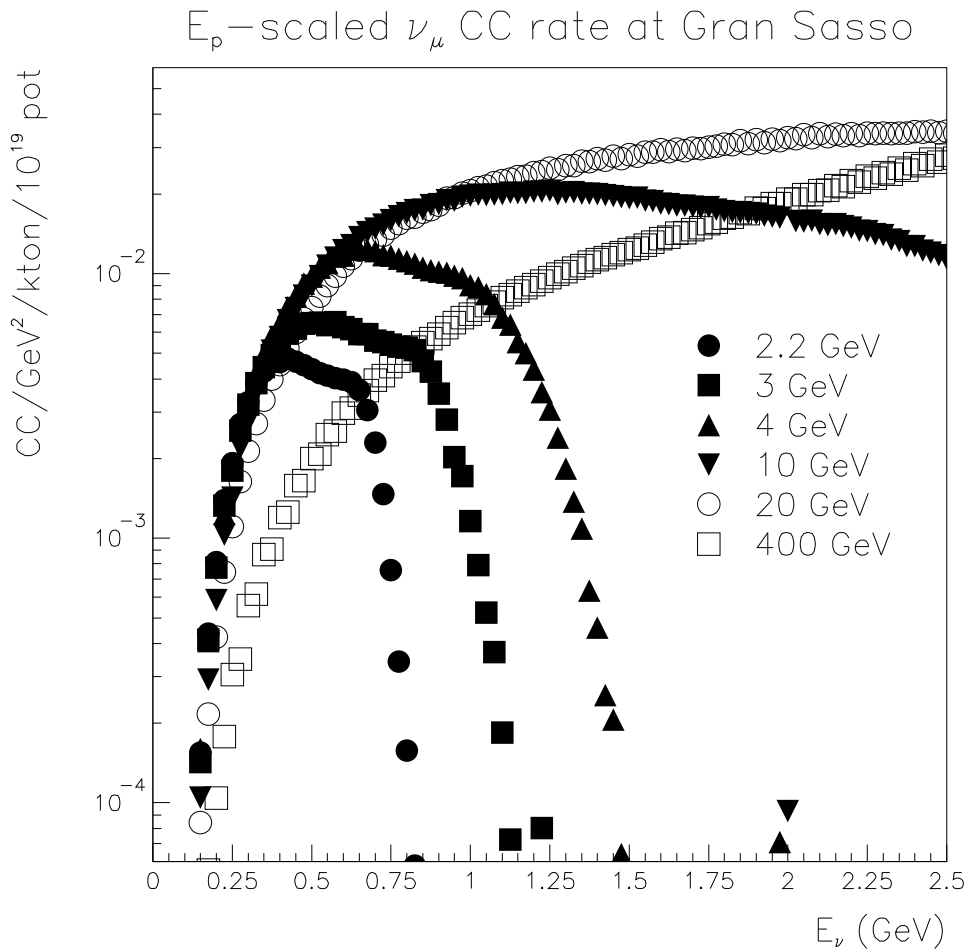


Figure 2: Rescaled energy spectrum of charged current events $N_{\nu_\mu, CC}(E_\nu)/E_p$ for various incident proton energies E_p (arbitrarily normalized to a baseline $L = 732$ km).

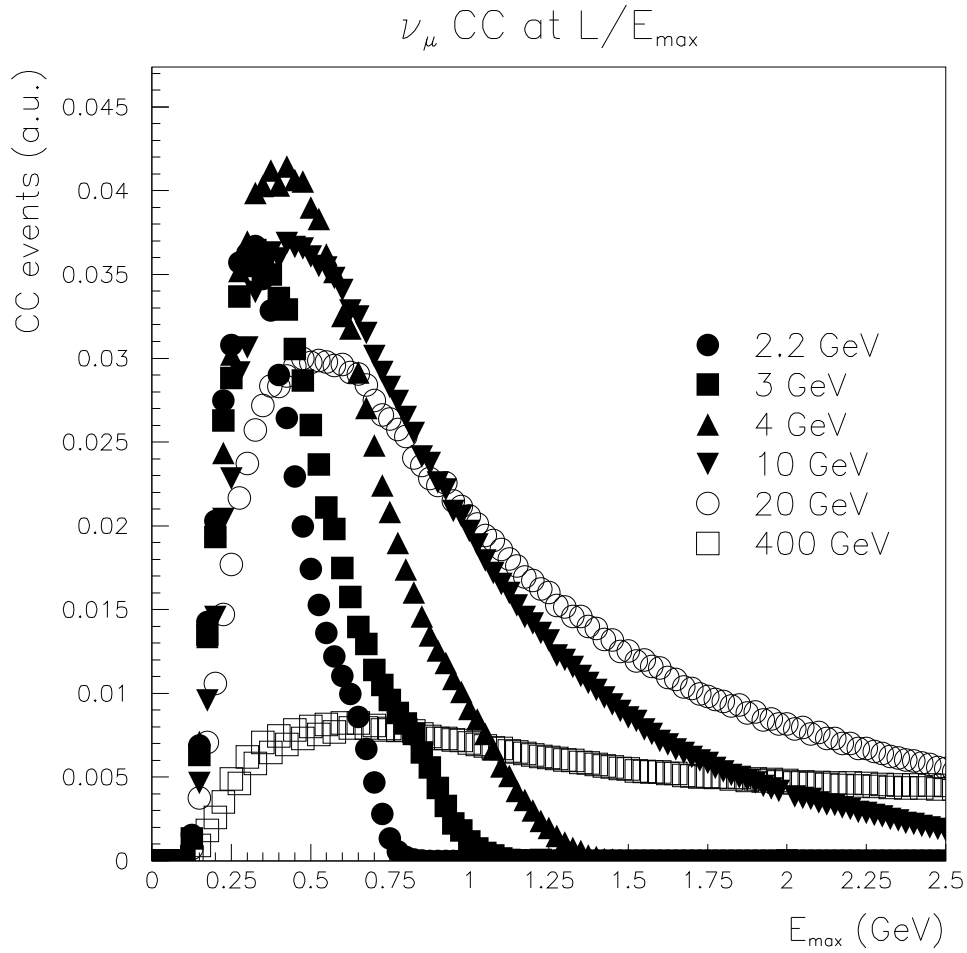


Figure 3: Doubly rescaled energy spectrum of charged current events $N_{\nu_\mu, CC}(E_\nu)/E_\nu^2/E_p$ for various incident proton energies E_p .

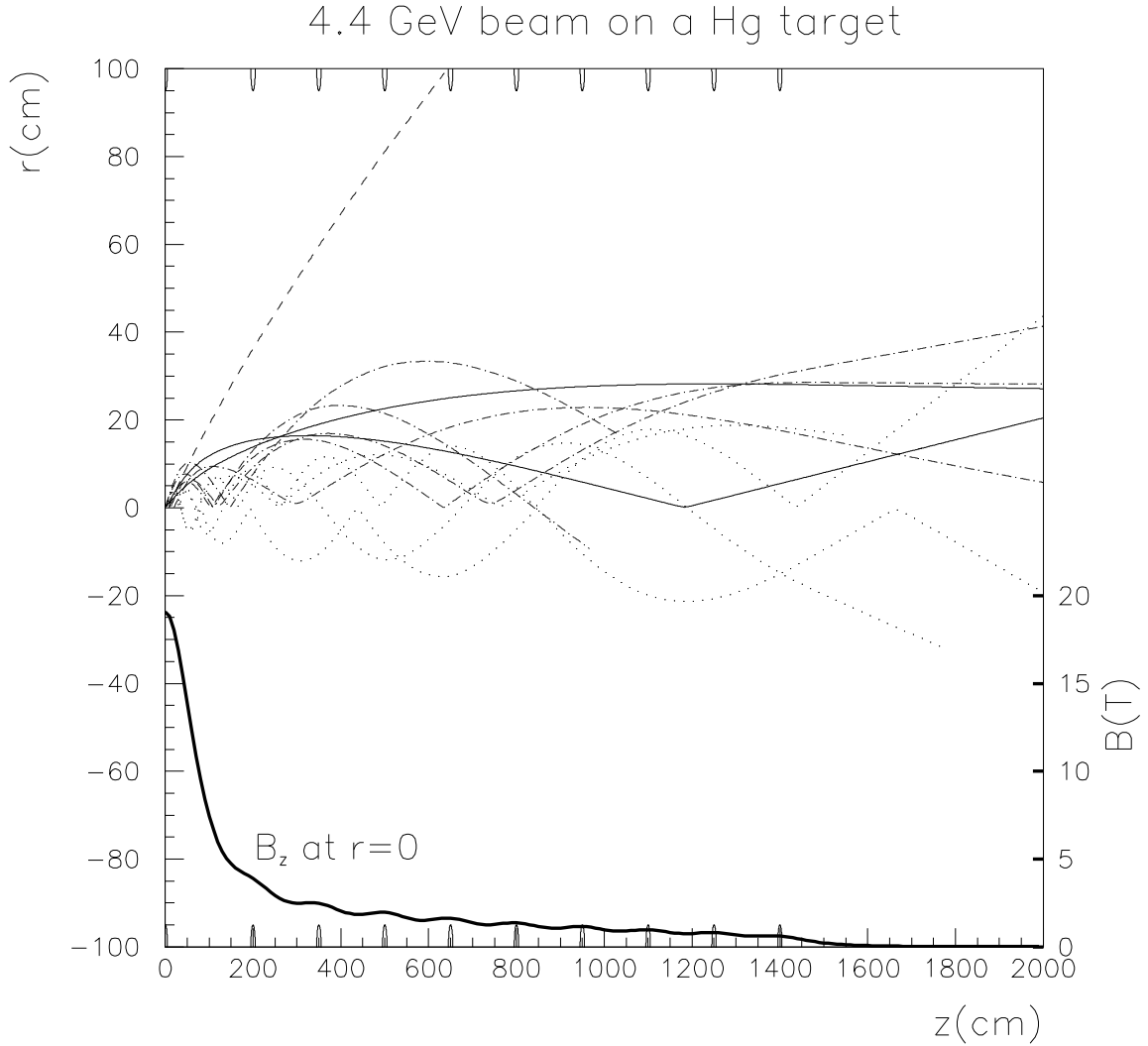


Figure 4: Particle trajectories in the current loops focusing, from a 4.4 GeV proton beam on a Hg target. Dotted tracks: $p_\pi < 0.5$ GeV, dot-dashed tracks $0.5 < p_\pi < 1$ GeV, continuous tracks $1 < p_\pi < 2$ GeV, dashed tracks $p_\pi > 2$ GeV. The thick curve is the on-axis magnetic field value (scale on the right). Loop positions are marked on top and bottom.

4.4 GeV beam

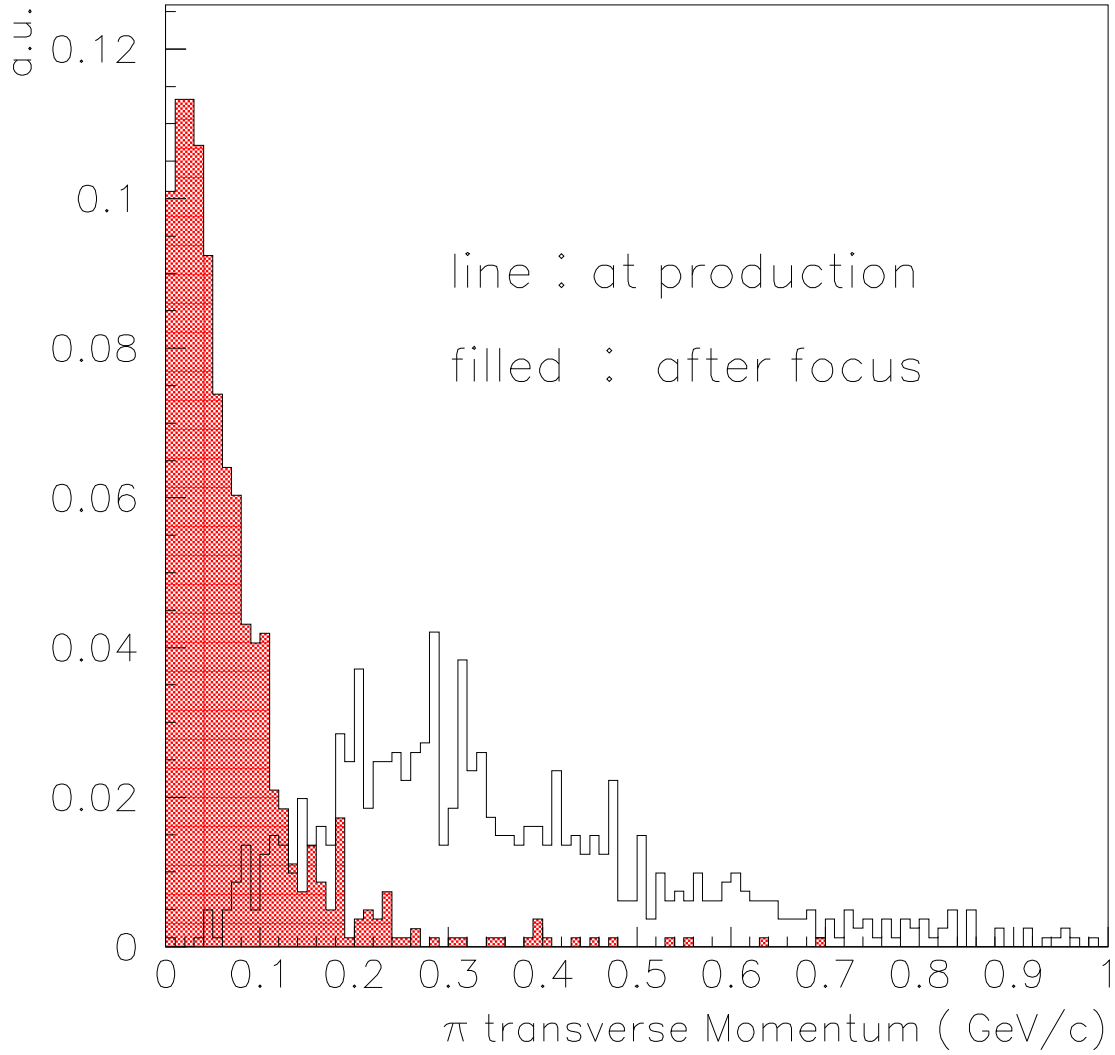


Figure 5: Effect of a multiple current loop system on the transverse momentum distribution, in the case of a 4.4 GeV beam on a mercury target

20 GeV beam

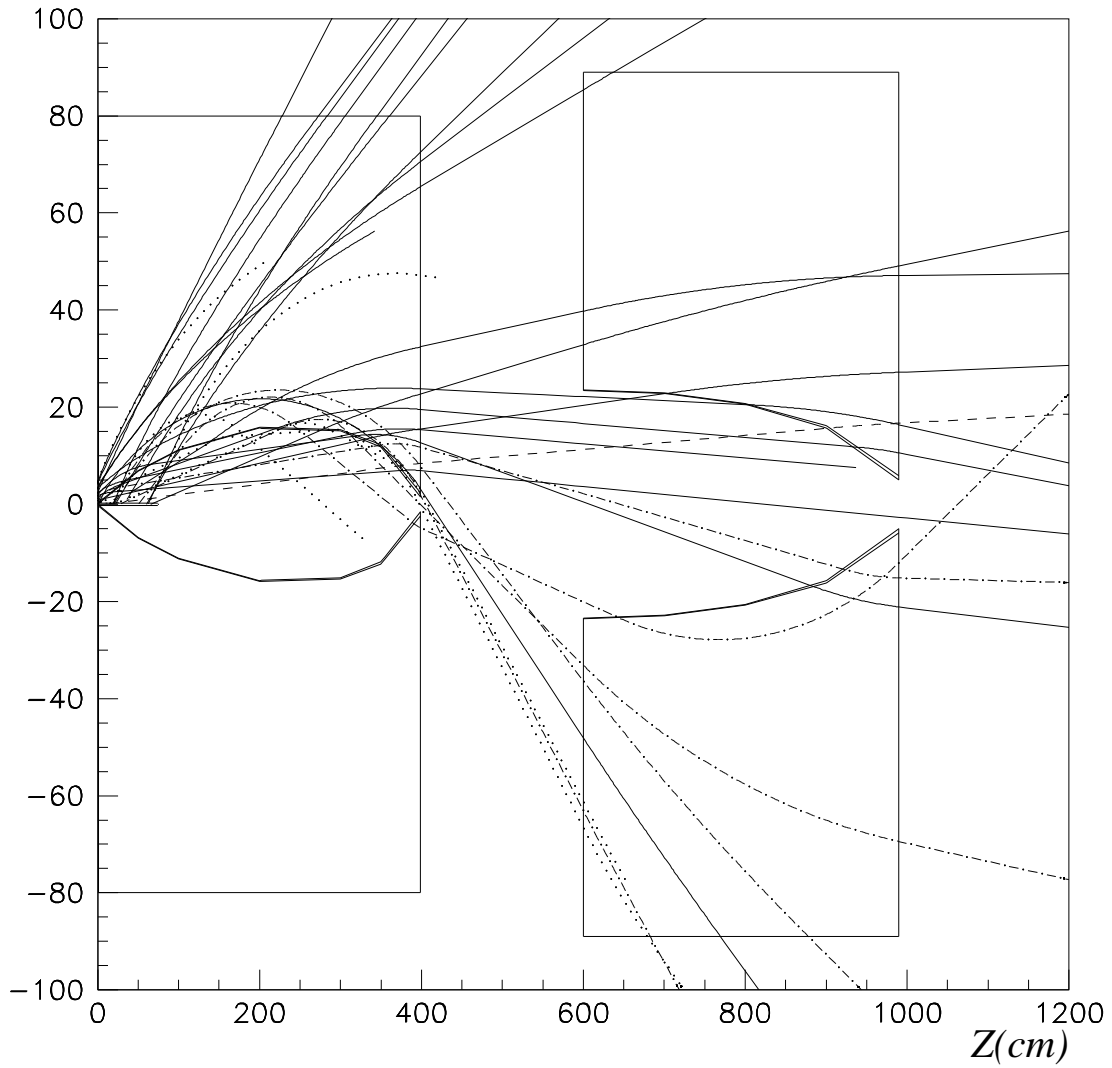


Figure 6: Particle trajectories in the horn+reflector focusing, from a 20 GeV proton beam on a C target. Dotted tracks: $p_\pi < 0.5$ GeV, dot-dashed tracks $0.5 < p_\pi < 1$ GeV, continuous tracks $1 < p_\pi < 6$ GeV, dashed tracks $p_\pi > 6$ GeV.

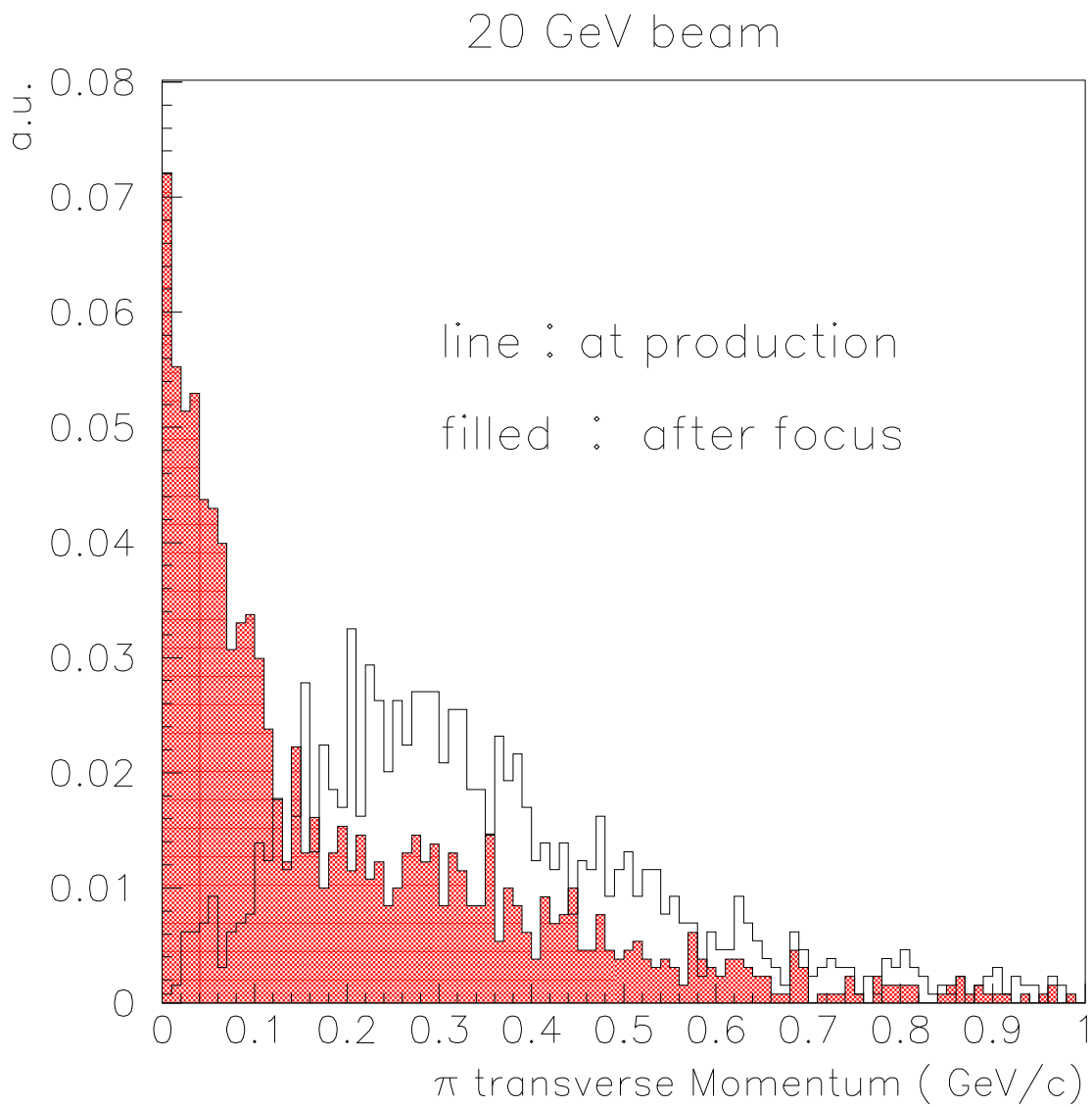


Figure 7: Effect of a double horn focusing on the transverse momentum distribution, in the case of a 20 GeV beam on a carbon target

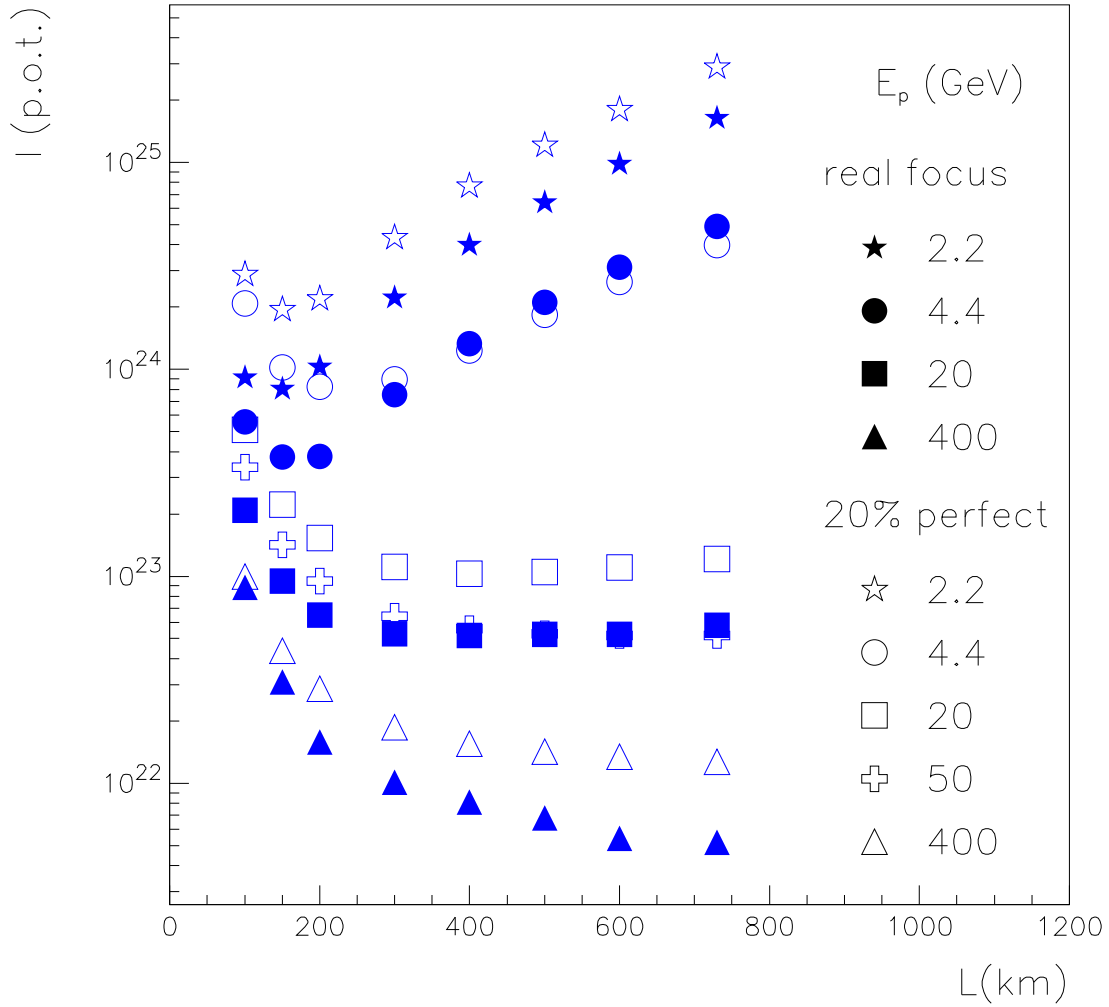


Figure 8: Integrated beam intensity needed to obtain 5 oscillated ν_e events in a 2.35 kton detector for $\Delta m^2 = 3 \times 10^{-3} \text{ eV}^2$ and $\sin^2(2\theta_{13}) = 10^{-3}$ for different beam energies and baselines. Full symbols correspond to the real focusing systems described in the text, open symbols to energy-independent 20% scaling from perfect focusing.

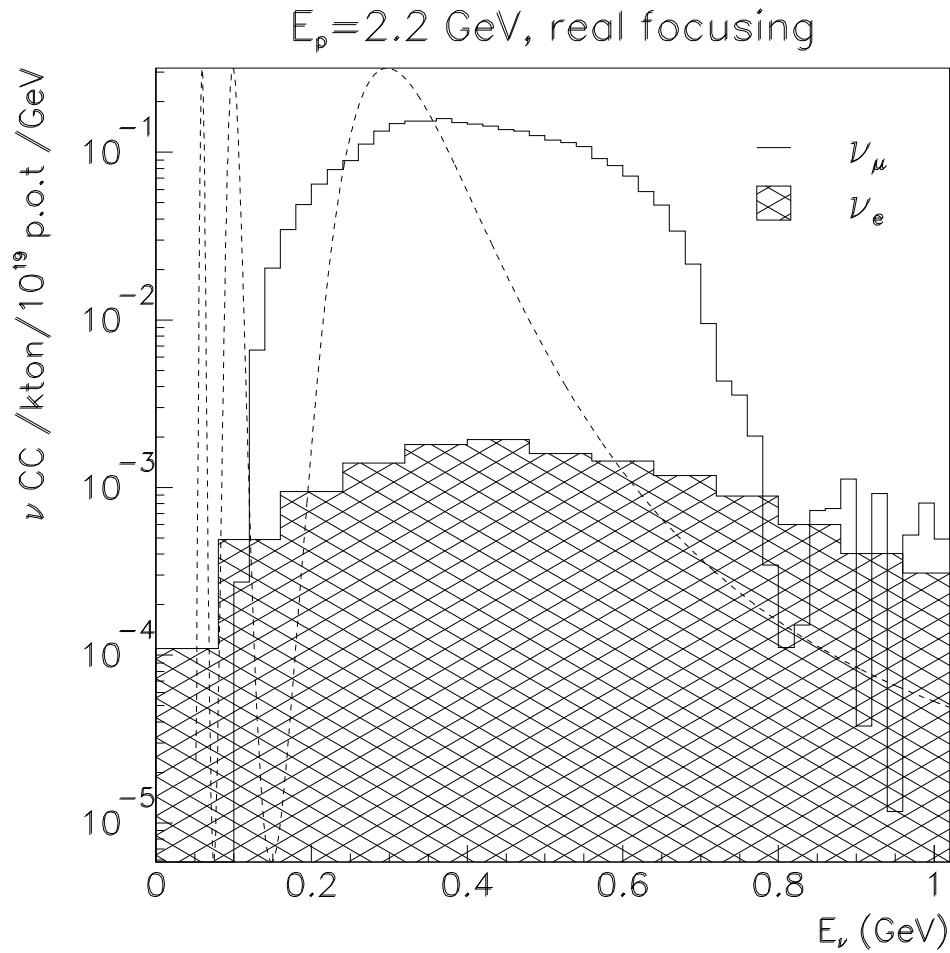


Figure 9: Charged current event rate at 120 km as a function of the neutrino energy computed with (real) coil focusing for 2.2 GeV proton energy. The dotted line corresponds to the oscillation probability (arb. norm.) for a $\Delta m^2 = 3 \times 10^{-3} \text{ eV}^2$.

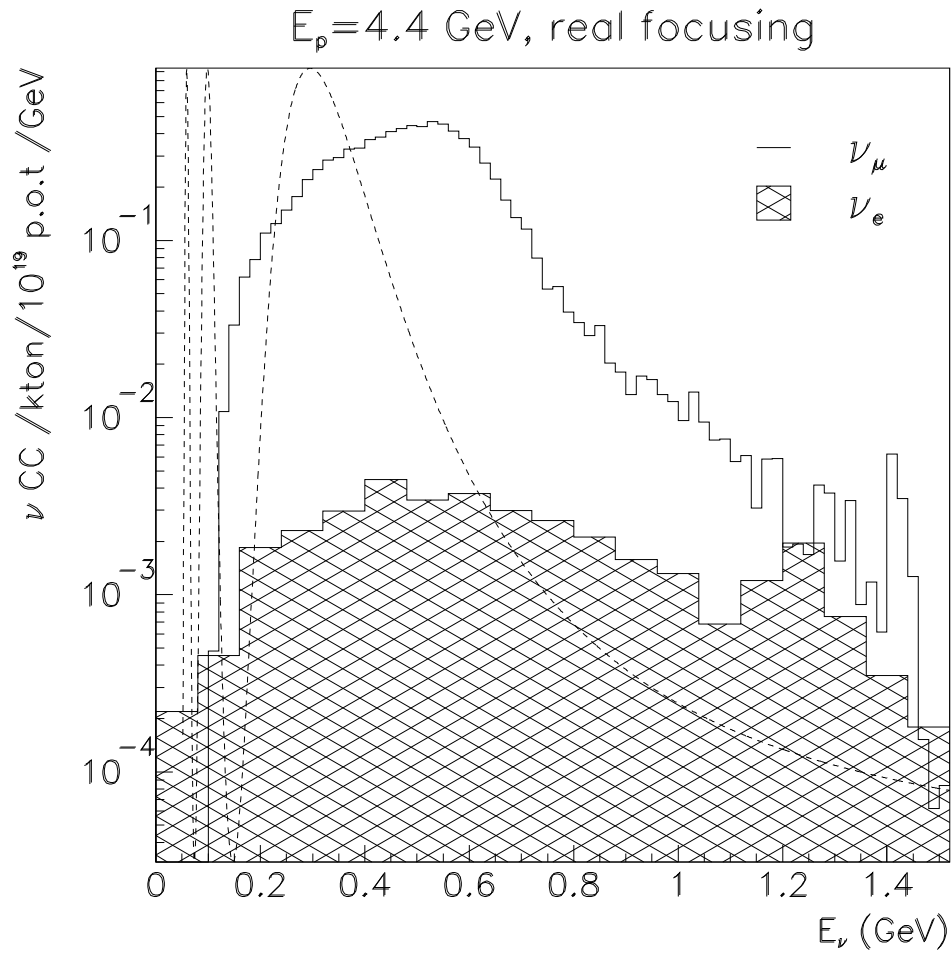


Figure 10: Charged current event rate at 120 km as a function of the neutrino energy computed with (real) coil focusing for 4.4 GeV proton energy. The dotted line corresponds to the oscillation probability (arb. norm.) for a $\Delta m^2 = 3 \times 10^{-3} \text{ eV}^2$.

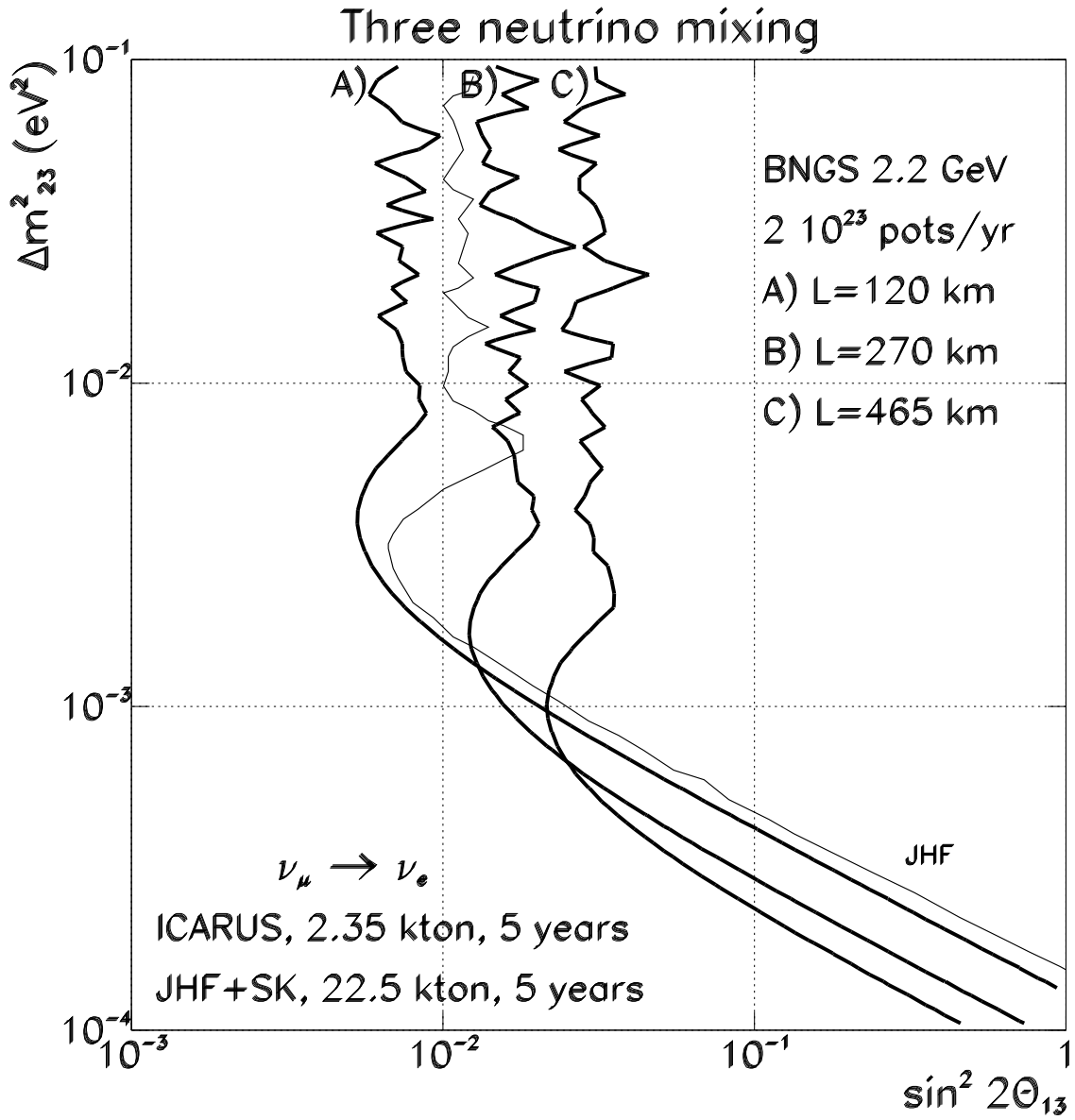


Figure 11: Expected 90% C.L. sensitivity to $\sin^2 2\theta_{13}$ mixing angle at 2.2 GeV proton energy for the three possible baselines $L = 120, 270$ and 465 km (thick lines), compared to expected results from JHF-SK[11] (thin line).

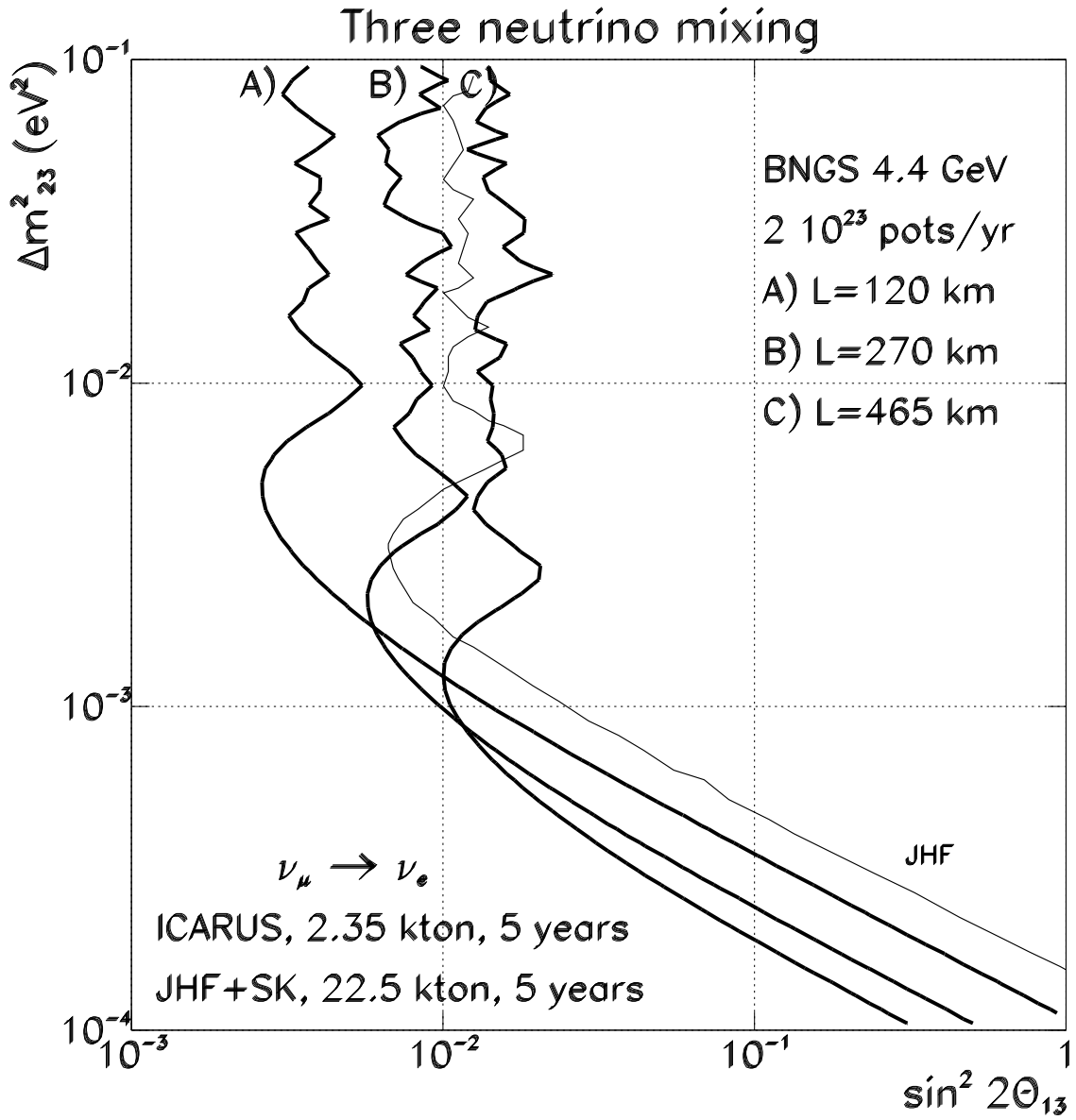


Figure 12: Expected 90% C.L. sensitivity to $\sin^2 2\theta_{13}$ mixing angle at 4.4 GeV proton energy for the three possible baselines $L = 120, 270$ and 465 km (thick lines), compared to expected results from JHF-SK[11] (thin line).

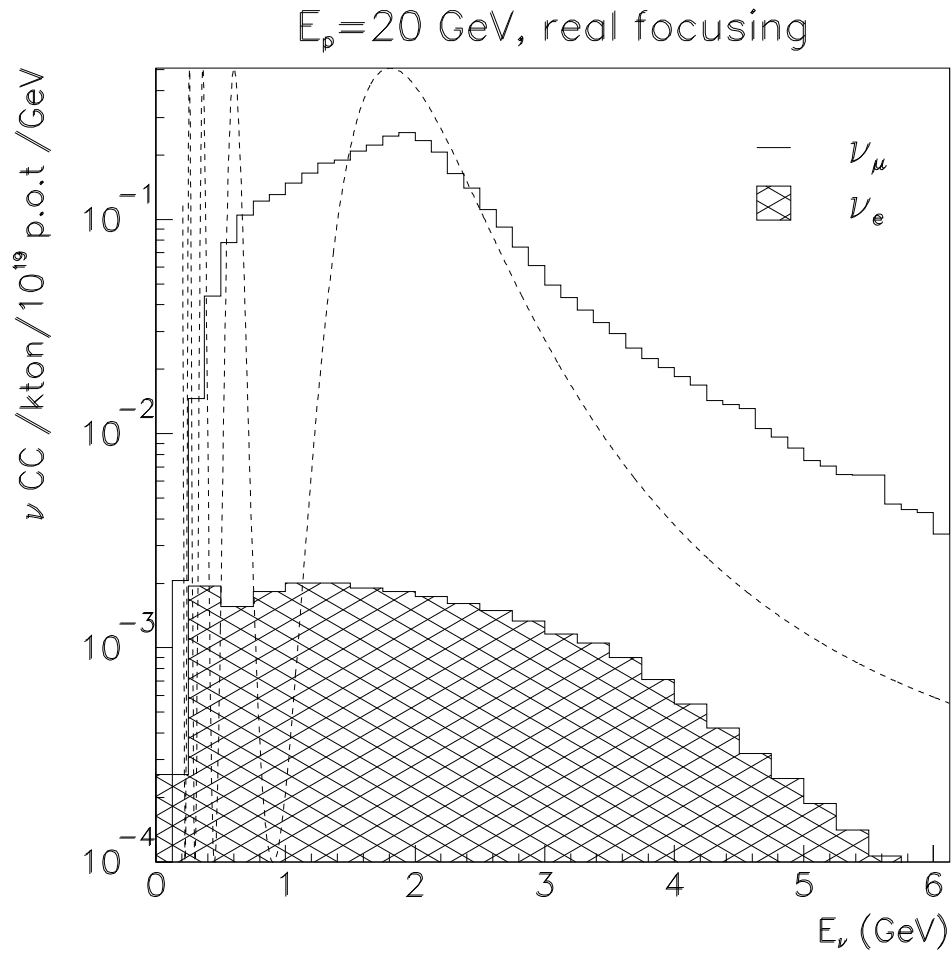


Figure 13: Charged current event rate at 730 km as a function of the neutrino energy computed with (real) horn focusing for 20 GeV proton energy. The dotted line corresponds to the oscillation probability (arb. norm.) for a $\Delta m^2 = 3 \times 10^{-3}$ eV².

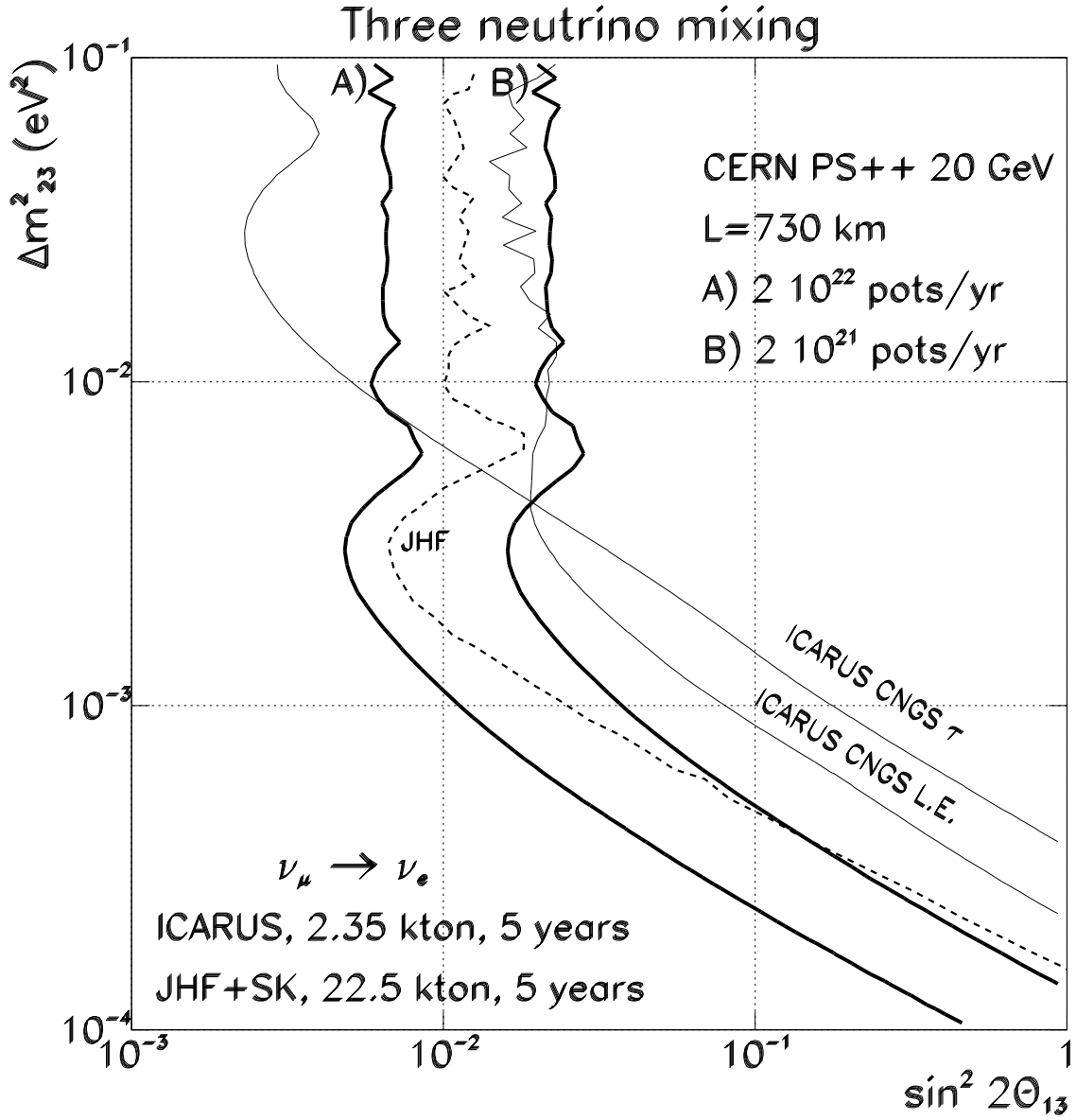


Figure 14: Expected 90% C.L. sensitivity to $\sin^2 2\theta_{13}$ mixing angle at 20 GeV proton energy for the CERN-LNGS baseline ($L=730$ km) (thick lines) for two yearly integrated proton intensities, compared to expected results from CNGS τ and L.E. optimized (See Ref.[12]) (thin lines) and JHF-SK[11] (dotted line).

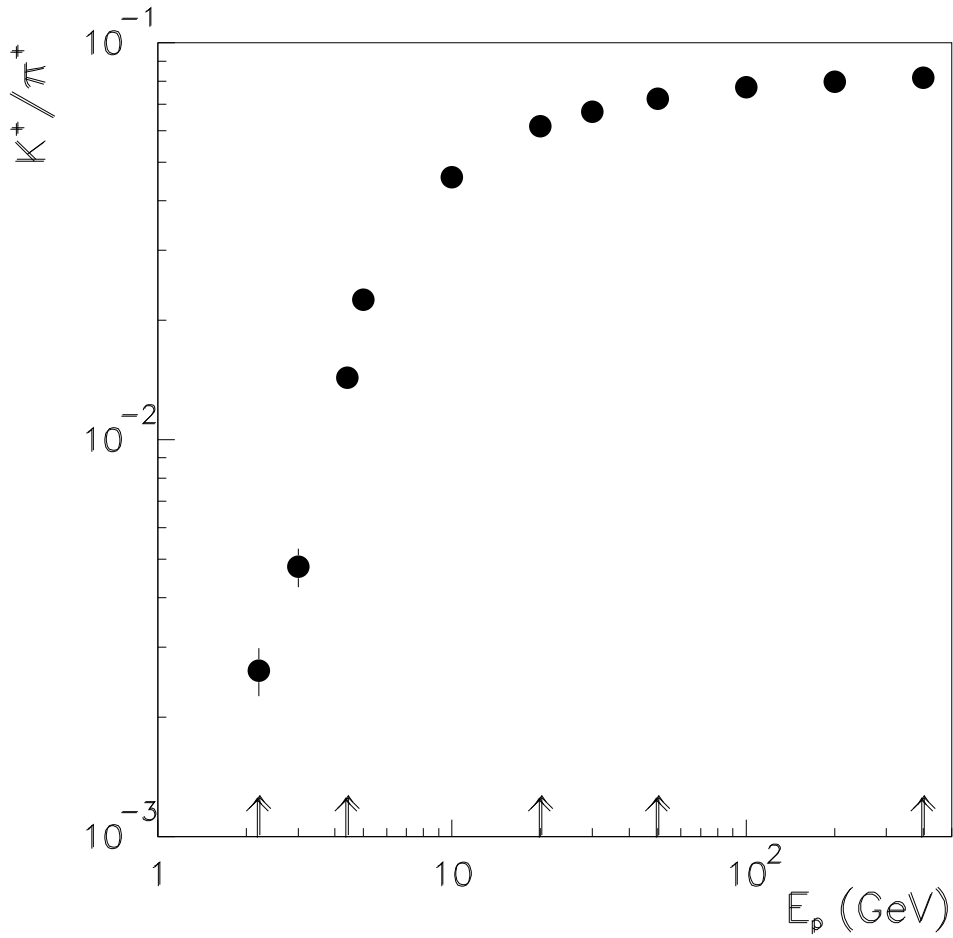


Figure 15: Expected ratio of charged K^+ to π^+ production as a function of the primary proton energy, for a 1m long, 2 mm radius graphite target. The arrows indicate proton energies of 2.2, 4.4, 20, 50 and 400 GeV.

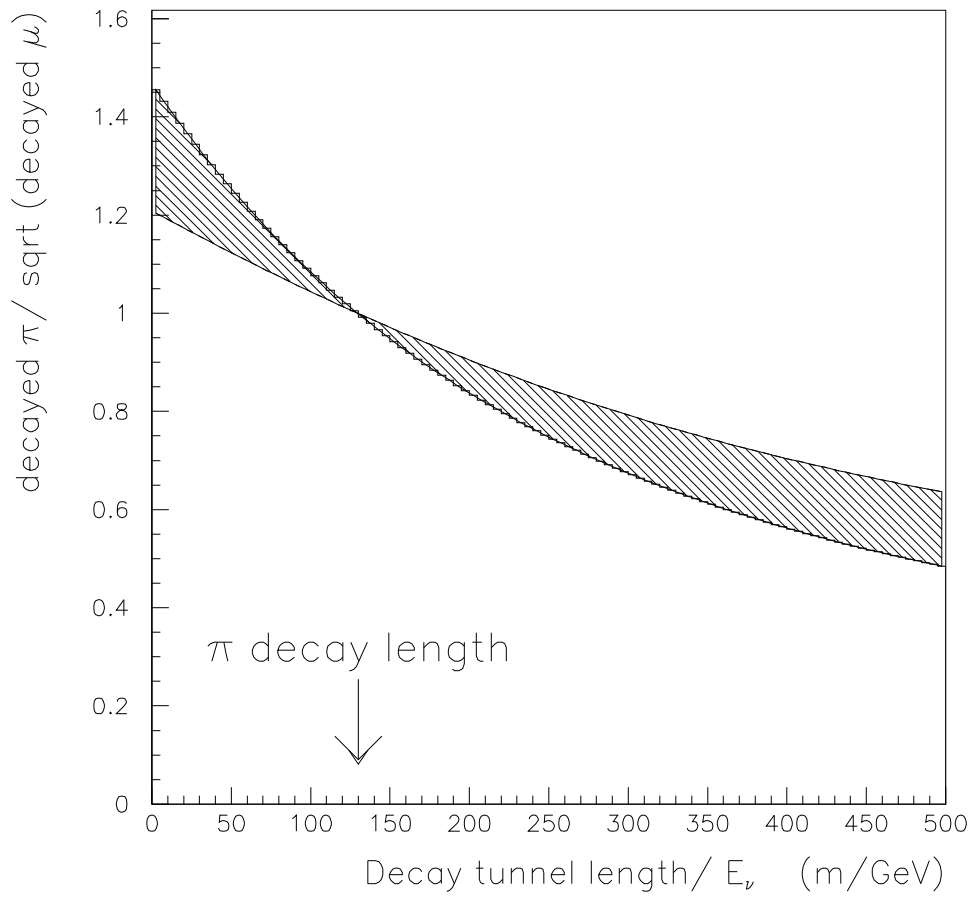


Figure 16: Ratio of pion decay over the square root of muon decay as a function of decay tunnel length, normalized to the value at one pion decay length.

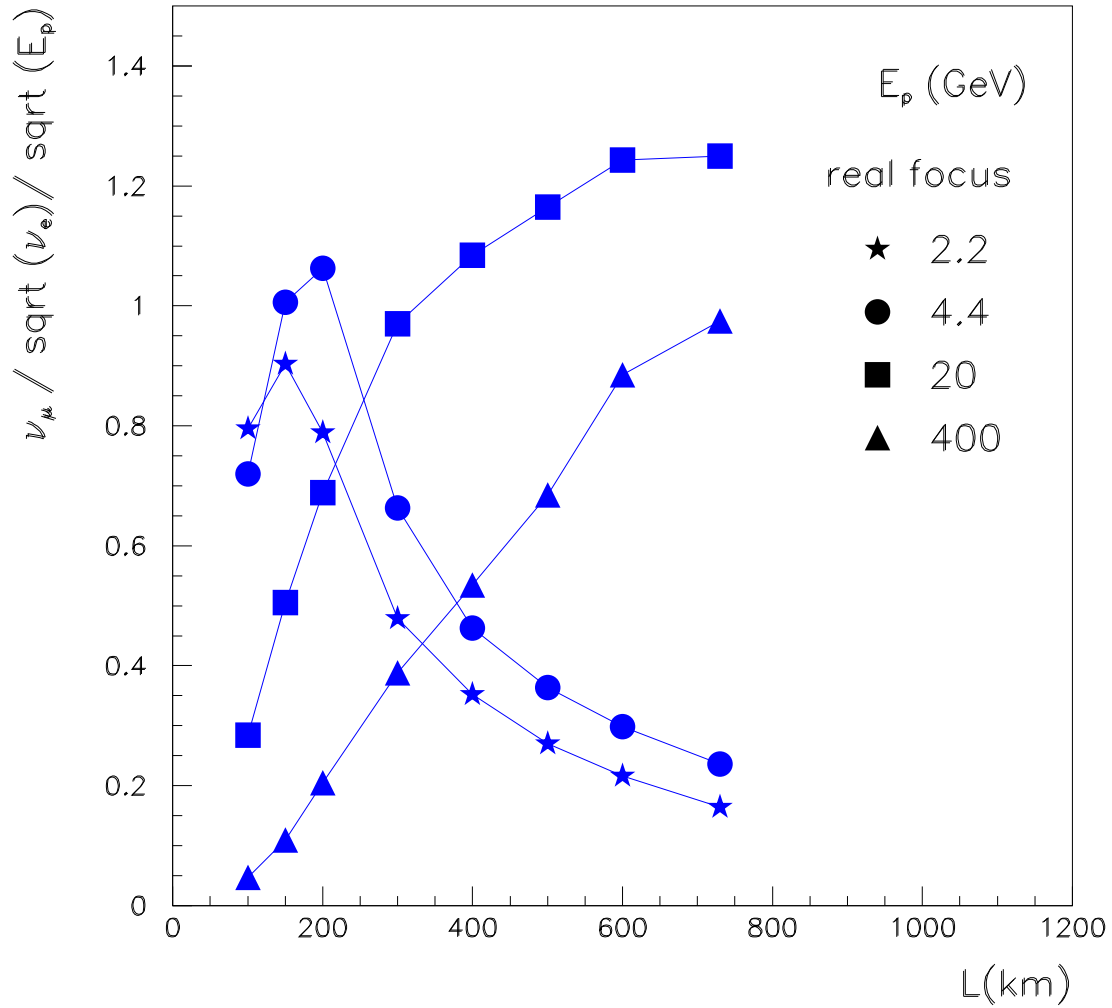


Figure 17: Rescaled ratio of muon neutrino flux over the square root of the electron neutrino flux divided by the square root of the proton energy (see text) $(\nu_\mu/\sqrt{\nu_e})/\sqrt{E_p}$ as a function of the baseline L .